

## CARBON AND OXYGEN ISOTOPIC RATIOS. II. SEMI-REGULAR VARIABLE M GIANTS

THOMAS LEBZELTER,<sup>1</sup> KENNETH H. HINKLE,<sup>2</sup> OSCAR STRANIERO,<sup>3</sup> DAVID L. LAMBERT,<sup>4</sup>  
CATHERINE A. PILACHOWSKI,<sup>5</sup> AND KRISTIE A. NAULT<sup>6</sup>

<sup>1</sup>*Department of Astrophysics, University of Vienna  
Türkenschanzstrasse 17, 1180 Vienna, Austria*

<sup>2</sup>*NSF's National Optical-Infrared Astronomy Research Laboratory  
P.O. Box 26732, Tucson, AZ 85726, USA*

<sup>3</sup>*INAF, Osservatorio Astronomico d'Abruzzo.  
I-64100 Teramo, Italy, and INFN-LNGS, Assergi (AQ), Italy*

<sup>4</sup>*W.J. McDonald Observatory and Department of Astronomy  
The University of Texas at Austin, Austin, TX 78712-1205, USA*

<sup>5</sup>*Astronomy Department, Indiana University Bloomington  
Swain West 319, 727 East Third Street, Bloomington, IN 47405-7105, USA*

<sup>6</sup>*Department of Physics & Astronomy, Univeristy of Iowa  
203 Van Allen Hall, Iowa City, IA 52242-1479, USA*

### ABSTRACT

Carbon and oxygen isotopic ratios are reported for a sample of 51 SRb- and Lb-type variable asymptotic giant branch stars. Vibration-rotation first- and second-overtone CO lines in 1.5 to 2.5  $\mu\text{m}$  spectra were measured to derive isotopic ratios for  $^{12}\text{C}/^{13}\text{C}$ ,  $^{16}\text{O}/^{17}\text{O}$ , and  $^{16}\text{O}/^{18}\text{O}$ . Comparisons with previous measurements for individual stars and with various samples of evolved stars, as available in the extant literature, are discussed. Using the oxygen isotopic ratios, the masses of the SRb stars can be derived. Combining the masses with Gaia luminosities, the SRb stars are shown to be antecedents of the Mira variables. The limiting parameters where plane-parallel, hydrostatic equilibrium model atmospheres can be used for abundance analysis of M giants are explored.

*Keywords:* stars: abundances — stars: evolution — stars: interiors — stars: variables: other — ISM: abundances stars: model atmospheres

### 1. INTRODUCTION

The upper giant branch is a decisive phase in the stellar evolution of low- and intermediate-mass stars. Large radial extension, low effective temperature, and stellar pulsation lead to significant mass loss. The material lost to the interstellar medium (ISM) in this way has been enriched by products of the stellar nucleosynthesis resulting from deep convective mixing (dredge-up). Therefore, these objects play an important role in the cosmic matter cycle. Abundance analysis of the surface composition probes the conditions and processes in the stellar interior.

The dredge-up replaces the primordial composition of the C, N, and O with the post-hydrogen-burning one. For the sun, the surface values are those of the presumed typical primordial gas,  $^{12}\text{C}/^{13}\text{C} = 89$  (Meibom et al. 2007),  $^{16}\text{O}/^{17}\text{O} = 2700$ , and  $^{16}\text{O}/^{18}\text{O} = 498$  (Lodders et al. 2009). The first major alteration of the surface composition occurs during the first dredge-up at the bottom of the red giant branch. Depending on the stellar parameters, further mixing events take place, in particular with the onset of double-shell burning on the asymptotic giant branch (AGB), the so-called third dredge-up.

thomas.lebzelter@univie.ac.at

khinkle@noao.edu

straniero@oa-teramo.inaf.it

This is our second Paper In a series to study the isotopic ratios of C and O in AGB stars. In the first paper of this series (Hinkle et al. 2016, Paper I) we presented an extensive discussion on the influence of stellar parameters and evolution on the isotopic ratios of these two key elements measured at the stellar surface. Here we confine the discussion to a brief summary of the main effects and refer to Paper I (note in particular Figure 10), Lebzelter et al. (2015a), and references therein for a more extensive description.

The CNO cycle depletes  $^{12}\text{C}$  and enhances  $^{13}\text{C}$ , a change that becomes visible as a steep drop in the  $^{12}\text{C}/^{13}\text{C}$  ratio down to 10 to 25 after the first dredge up. A slight dependence of the resulting ratios on stellar mass is expected, with the more massive stars showing higher  $^{12}\text{C}/^{13}\text{C}$  values (Paper I). Extensive observational evidence (e.g. Charbonnel et al. 1999) exists that extra-mixing along the red giant branch (RGB) can further reduce the ratio between the two carbon isotopes by a factor of two in low-mass stars. The interplay between production, mixing, and destruction of the various oxygen isotopes results in a dependence of  $^{16}\text{O}/^{17}\text{O}$  on stellar mass (Boothroyd et al, 1994; El Eid 1994; Karakas & Lattanzio 2014), with the isotopic ratio decreasing with increasing mass as different depths and thus different regions of  $^{17}\text{O}$  enhancement are reached by the first dredge-up.  $^{18}\text{O}$ , on the other hand, is depleted by H burning and therefore  $^{16}\text{O}/^{18}\text{O}$  is increasing with the first dredge-up. This effect, however, is almost independent of mass.

The second dredge-up has only a mild effect on the isotopic ratios on the surface. With the third dredge-up episodes, which are predicted to occur in stars with main-sequence masses between approximately 1.3 and  $5 M_{\odot}$  at solar metallicity,  $^{12}\text{C}/^{13}\text{C}$  is strongly enhanced, while there is little effect on the oxygen isotopic ratios. In the more massive AGB stars, Hot Bottom Burning (HBB) can effect the oxygen isotopes, in particular the abundance of  $^{18}\text{O}$  which is significantly depleted (Lattanzio et al. 1996). As pointed out by Lebzelter et al. (2015a), the  $^{16}\text{O}/^{18}\text{O}$  is good indicator of the primordial  $^{18}\text{O}$  abundance in a star, so that star-to-star variations of this ratio also includes information on the primordial abundance scatter of this isotope.

Isotopic ratios of abundant elements like C and O thus provide a valuable and easily accessible tool to study the evolution of low- and intermediate-mass stars along the AGB and to get access to the main-sequence mass and the primordial composition of these objects. The usage of this method has a long tradition in astrophysics going back to the 1970s (Dearborn 1977). In particular, the  $^{12}\text{C}/^{13}\text{C}$  ratio was measured for a large number of objects with various methods. Oxygen isotopic ratios received less attention until the landmark papers by Harris & Lambert (1984b), Harris et al. (1985), and Smith & Lambert (1990). These advances resulted from the advent of high-resolution near-infrared spectroscopy in stellar astrophysics. Measurements in the radio regime (e.g. Ramstedt & Olofsson 2014) and in the far-infrared (e.g. Justtanont et al. 2015) extended the possibilities for studies of isotopic ratios in evolved stars in the past years.

Very high precision isotopic ratios can be determined from presolar grains. Comparing the results from such grains with model predictions has allowed us to identify the kind of stars from which they originated (Zinner 1998; Nittler 2009). We know that most O-rich presolar grains were formed in the cool circumstellar envelope around red giants stars lived before the birth of the solar system. However, a comparison of predictions with isotopic ratios derived from measurements in stars is still incomplete. This Paper Is part of our effort to close this gap and to derive isotopic ratios of carbon and oxygen for evolved low- and intermediate-mass stars.

In such stars, isotopic ratios can be studied spectroscopically owing to the isotopic shifts between the isotopologues of the abundant molecule CO. Vibration-rotation molecular transitions well suited for this task are found in the near-infrared range between 1 and  $5 \mu\text{m}$ . In K, M, S, and C giants the low stellar effective temperature results in spectral lines of sufficient strength to detect the less abundant isotopologues.

Previous studies dealt with small samples of stars or focused on only one or two of the three isotopic ratios mentioned above. In our series of papers, we aim at determining all three isotopic ratios for a large sample of AGB stars in a homogeneous and self-consistent way. With this data set, our goal is to systematically compare model predictions with observations, describe the population on the AGB more properly in terms of mass, and effectively contrast the results from presolar grains with the atmospheres of the dust producers, namely, the AGB stars. Our project is restricted to oxygen-rich stars, i.e. spectral type M and S. Carbon-rich stars present a unique set of issues resulting largely from the very rich spectrum. Studies on large samples have previously been published (e.g. Lambert et al. 1986; Abia et al. 2017).

Most, if not all, AGB stars are variable, forming the group of long period variables (LPVs). Their pronounced variability, brightness, and red color provide good indicators to identify these objects in the sky. However, as the final evolutionary stage for stars in a wide initial mass range, the AGB population of the Galactic field is highly inhomogeneous in terms of mass, age, composition, and variability characteristics. Based on the latter, LPVs are

typically divided into types M (miras), SRa and SRb variables, with the first two groups having large-amplitude light variations with pronounced periodicity, while the third group is characterized by smaller light amplitudes and phases of irregularity. For the first paper of this series (Paper I) we derived carbon and oxygen isotopic ratios for a group of Mira and SRa variables. These stars were attractive candidates in the context of the galactic evolution, because they have prodigious mass loss and are certain to be on the AGB, presumably near the tip. The isotopic ratios of C and O indicated that the majority of the M-star miras and SRa variables have main-sequence masses of  $\leq 2 M_{\odot}$ .

The present Paper Is a study of the C and O isotopes in small-amplitude variables, primarily in the SRb class. In Section 2 we describe the sample for this study, the observational methods, and the applied steps of the data reduction. Sects. 3 and 4 present the results for the SRb variables including a relation between the CO excitation temperature and the effective temperature of a star. We use this relation and Gaia distances to constrain atmospheric models for targets and compare isotopic ratios of oxygen determined by curve-of-growth analysis and by spectrum synthesis. The paper closes with a discussion of the findings (Section 5).

## 2. OBSERVATIONS AND REDUCTIONS

### 2.1. Sample

As was the case for Paper I, the spectroscopic material analyzed here is drawn entirely from the archives of the Kitt Peak National Observatory (KPNO) 4-meter Mayall Telescope Fourier Transform Spectrometer (FTS). For this paper the sample is mainly M and S SRb stars. The variable type was obtained from the latest General Catalog of Variable Stars (GCVS). In addition to SRb variables, the GCVS class of some program stars is Lb. These two variable classes have similar, if not identical, characteristics (see [Lebzelter, & Obbrugger 2009](#)). In addition, we included two stars classified as SRa (GZ Peg and DY Gem) and two as SRc (Y Lyn and  $\delta^2$  Lyr) that are in the FTS archive. GZ Peg has a GCVS amplitude of less than 0.3 mag and thus belongs to variability class SRb rather than to SRa. A light curve of the star could not be found in the literature. For DY Gem, an ACVS light curve ([Pojmanski et al. 2005](#)) exists that shows very obvious signs of irregularity. The amplitude of the main period is rather small, but the star may have a long secondary period. We believe that DY Gem can be considered an SRb. The two SRcs are, if classified correctly, supergiants, and thus not AGB stars. The classification of Y Lyn as an SRc is based on its spectroscopic luminosity class Ib-II ([Keenan 1942](#)). However, in various papers Y Lyn is discussed in the course of AGB stars. [Guandalini, & Busso \(2008\)](#) derived a luminosity in accordance with the values they found for miras. For  $\delta^2$  Lyr luminosity class II was confirmed in the extensive study of supergiants by [Levesque et al. \(2005\)](#). Therefore, we assume that the classification as SRc is correct. We decided to derive isotopic ratios for these stars within the present paper, but we handle them separately in the discussion. The complete set of spectra used for this project is listed in Table 1. For all the sample stars spectra were present in the archive that cover both the *H* and *K* windows.

The archival spectra were originally observed for a variety of projects including abundance studies. We will refer to these former studies when comparing our findings with values from the literature (Section 4.2). Unlike the time series in Paper I, the current data set consists mainly of individual observations. Where multiple spectra of a star existed, we typically analyzed those with signal-to-noise ratio (S/N)  $\gtrsim 50$  and used the one with the highest S/N ratio for the abundance results. The other spectra were used as an estimate of the uncertainties.

**Table 1.** Observations

HD	HR/BD	Var Name	Var Type <sup>a</sup>	Date	Res. (cm <sup>-1</sup> )	S/N K peak	S/N H
6860	HR 337	$\beta$ And	var	76 Jun 6	0.08	$-^b$	
6860	HR 337	$\beta$ And	var	79 Jun 14+15	0.04	128	
7351	HR 363	DT Psc	SR:	77 Jun 29	0.17	83	
18191	HR 867	RZ Ari	SRb	76 Aug 17	0.09	89	
18884	HR 911	$\alpha$ Cet	Lb:	76 Sep 28	0.08	74	
20720	HR 1003	$\tau^4$ Eri	Lb	76 Sep 29	0.09	65	
22649	HR 1105	BD Cam	Lb	76 May 14	0.21	107	

**Table 1** continued on next page

**Table 1** (*continued*)

HD	HR/BD	Var Name	Var Type <sup>a</sup>	Date	Res. (cm <sup>-1</sup> )	S/N K peak	S/N H
30959	HR 1556	o <sup>1</sup> Ori	SRb	76 Aug 23	0.08	73	
30959	HR 1556	o <sup>1</sup> Ori	SRb	78 Jan 22	0.10	73	
39225	HR 2028		var	89 Sep 14	0.10	85	49
44478	HR 2286	$\mu$ Gem	Lb	76 Sep 29	0.08	30	
44478	HR 2286	$\mu$ Gem	Lb	79 Sep 5+7+9	0.04	268	
49368		V613 Mon	SRb:	87 Apr 14	0.07	61	25
55966	HR 2742	VZ Cam	Lb:	90 Apr 12	0.07	149	65
58521		Y Lyn	SRc	78 Jan 22	0.10	81	
64332		NQ Pup	Lb	87 Apr 13	0.07	56	29
71250	HR 3319	BP Cnc	SRb	78 Oct 15	0.09	63	
94705	HR 4267	VY Leo	Lb:	90 Apr 11	0.07	67	34
96360		HL UMa	SRb	87 Apr 14	0.07	64	30
100029	HR 4434	$\lambda$ Dra	SR	90 Apr 12	0.07	98	53
102212	HR 4517	$\nu$ Vir	SRb	82 Apr 8	0.07	100	86
106198	HR 4647	V335 Hya	Lb	87 Apr 13	0.07	111	61
112300	HR 4910	$\delta$ Vir	SR	76 Jun 18	0.09	55	
112300	HR 4910	$\delta$ Vir	SR	77 Jun 24	0.09	70	
114961		SW Vir	SRb	76 Jun 18	0.09	64	
119228	HR 5154	IQ UMa	SRb	90 Apr 11	0.07	82	50
121130	HR 5226	CU Dra	Lb:	77 Jun 28	0.09	64	
123657	HR 5299	BY Boo	Lb:	76 Aug 18	0.09	32	
126327		RX Boo	SRb	76 Jan 14	0.09	64	
132813	HR 5589	RR UMi	SRb	76 Aug 18	0.08	58	
133216	HR 5603	$\sigma$ Lib	SRb	76 Aug 18	0.08	94	
146051	HR 6056	$\delta$ Oph	var	77 Jun 24	0.09	62	
148783	HR 6146	g Her	SRb	77 Jun 30	0.09	90	
149683		R UMi	SRb	83 Sep 13	0.07	98	
154143	HR 6337		var	90 Apr 12	0.07	149	65
163990	HR 6702	OP Her	SRb	76 Sep 29	0.08	43	
168574	HR 6861	V4028 Sgr	SR:	76 Sep 29	0.09	43	
175588	HR 7139	$\delta$ 2 Lyr	SRc:	76 Apr 11	0.09	91	
175865	HR 7157	R Lyr	SRb	90 Apr 11	0.07	168	93
182917		CH Cyg	SR+Z And	79 Feb 8	0.08	133	
183439	HR 7405	$\alpha$ Vul	var	76 May 16	0.18	89	
184313		V450 Aql	SRb	84 Feb 21	0.07	76	
184313		V450 Aql	SRb	84 Nov 13	0.07	85	
196610	HR 7886	EU Del	SRb	90 Apr 12	0.07	81	35
198026	HR 7951	EN Aqr	Lb	76 May 16	0.16	51	
198164		CY Cyg	Lb	76 Jun 19	0.23	52	
200527	HR 8062	V1981 Cyg	SRb	87 Apr 13	0.07	86	53
202369	HR 8128	29 Cap	var?	76 May 12	0.18	90	
205730	HR 8262	W Cyg	SRb	77 Apr 4	0.10	54	
205730	HR 8262	W Cyg	SRb	84 Apr 8	0.07	113	
209872		SV Peg	SRb	83 May 21	0.07	81	
209872		SV Peg	SRb	84 Nov 13	0.07	107	
216386	HR 8698	$\lambda$ Aqr	Lb	76 Jun 6	0.08	64	

**Table 1** *continued on next page*

Table 1 (continued)

HD	HR/BD	Var	Var	Date	Res.	S/N K	S/N H
		Name	Type <sup>a</sup>		(cm <sup>-1</sup> )	peak	
216672	HR 8714	HR Peg	SRb	77 Jun 4	0.17	115	
216672	HR 8714	HR Peg	SRb	88 Jul 2	0.04	67	
217906	HR 8775	$\beta$ Peg	Lb	76 May 12	0.09	105	
218634	HR 8815	GZ Peg	SRa	77 Jun 4	0.17	– <sup>b</sup>	
224935	HR 9089	YY Psc	Lb:	76 Jun 18	0.09	31	
260297		DY Gem	SRa	87 Apr 14	0.07	93	37
	BD+48 1187	TV Aur	SRb	77 Aug 25	0.08	56	
	BD+48 1187	TV Aur	SRb	87 Apr 14	0.07	62	24

<sup>a</sup>Variable class from GCVS

<sup>b</sup>Only one scan, no difference spectrum

## 2.2. Observations

A description of the FTS can be found in Paper I as well as in [Pilachowski et al. \(2017\)](#). In summary, the FTS was operated between the years 1975 and 1995 by KPNO as a coude instrument on the Mayall Telescope ([Hall et al. 1979](#)). The FTS was a nearly perfect spectrograph for observing bright objects. Fourier spectrometers have very large wavelength coverage, no scattered light, and a well-defined instrumental profile. The broad wavelength coverage resulted in a highly useful archive.

The program spectra consist of observations covering the 1.5 to 2.5  $\mu\text{m}$  ( $H$  &  $K$ ) spectral region. The  $H$  window covers the weaker CO  $\Delta v=3$  lines while the long-wavelength side of the  $K$  window covers the CO  $\Delta v=2$  bands. This provides a range of line strengths for the common isotopologue. In the previous paper the observations were limited to those made with a single pair of detectors with matching filters. In this paper this has been broadened to include spectra utilizing a dichroics with spectra taken through separate  $H$  and  $K$  filters. The wavelength bounds of the spectra are the same, with the main difference being the details of the filter response.

The natural unit of an FTS is inverse wavelength, i.e. wavenumber ( $\sigma$ ) and in standard convention these are  $\text{cm}^{-1}$  units. The spectral resolution ( $R = \sigma/\Delta\sigma$ ) is constant in wavenumber. High-resolution spectra taken with the 4 meter FTS typically have a resolution of  $\sim 0.070 \text{ cm}^{-1}$ . This corresponds to  $R \sim 57000$  at the red end ( $4000 \text{ cm}^{-1} = 2.5 \mu\text{m}$ ) of the spectrum and  $R \sim 96000$  at the blue end ( $6670 \text{ cm}^{-1} = 1.5 \mu\text{m}$ ). FTS spectra are typically apodized to dampen the sidelobes of the sinc function instrumental profile. Damping the amplitude of the instrumental profile sidelobes lowers the resolution and results in a corresponding increase in signal-to-noise. All spectra discussed here have been apodized by function I2 of [Norton & Beer \(1976\)](#).

The FTS generated two interferograms for each observation. The resulting spectra are identical except for the noise. The S/N values appearing in Table 1 are the RMS of the difference compared to the peak signal. For late-type stars the peak signal for observations covering the  $K$  and  $H$  band simultaneously always occurs in the  $K$ -band. For observations taken with the dichroic we present separate  $H$ - and  $K$ -band S/N.

## 2.3. Telluric correction

The technology used for the FTS was suitable for bright stars. The high-resolution  $K$ -band limit was  $\sim +4$ . Most of the stars in our sample are brighter. The intrinsic colors of M stars have  $K - V > 3$  ([Tokunaga 2002](#)). Since the intrinsic colors of hot stars have  $K - V \sim 0$  it is clearly very difficult to find a suitably bright telluric reference star for a bright M giant. As a result, most FTS spectra do not have an associated telluric reference star. Furthermore, the FTS spectra do not have meta-data providing information about the weather conditions. In the past we have not attempted any telluric correction and relied entirely on the large number of molecular lines present in the very large FTS bandpass. However, the rare oxygen CO isotopologues do not have that many available lines. The situation is tractable for  $^{12}\text{C}^{17}\text{O}$  since the 2-0 band has a conspicuous series of lines in spaces between telluric lines from 4280 to 4295  $\text{cm}^{-1}$ . But no such region exists for  $^{12}\text{C}^{18}\text{O}$ . For this isotopologue we have to rely on isolated lines. In an attempt to reduce blending and increase the selection of lines, we have corrected the most important oxygen isotope

regions for telluric absorption using synthetic telluric spectra. The suite of available options is discussed by Seifahrt et al. (2010). We selected the ATRAN tool (Lord 1992) because of its simplicity. Our technique is to estimate airmass and precipitable water from the 4511 - 4516  $\text{cm}^{-1}$  region. This region has minimal stellar lines with isolated  $\text{H}_2\text{O}$  and  $^{12}\text{CH}_4$  telluric lines. Based on these estimates for airmass and precipitable water we applied a telluric correction to the oxygen isotope regions. The correction is relatively crude, for instance, we have not attempted to modify the telluric atmosphere for temperature, but nonetheless the method satisfactorily removes unsaturated telluric lines.

### 3. STELLAR PARAMETERS

#### 3.1. *Effective Temperatures and CO Excitation Temperatures*

In Paper I isotopic abundances were derived using a simple curve-of-growth technique. This is a robust technique for determining isotopic ratios. It relies on a small number of assumptions by comparing lines of similar depths. As the first step in the current analysis we have employed this technique. The excitation temperature of the weak CO lines, which directly affects the isotopic ratios, was extracted by forcing high- and low-excitation lines with the same observed equivalent width to the same location on the curve of growth (Hinkle et al. 1976). We used the same technique in Paper I to derive isotopic ratios from the spectra of mira stars. FTS spectra are perfectly suited for the application of this technique because of the large wavelength coverage. In the 1.5 - 2.5  $\mu\text{m}$  region of late-type stars the large number of CO lines observed results in a well-defined curve of growth. This wavelength region spans CO first and second overtones and the large range in oscillator strength makes possible the measurement isotope ratios spanning three orders of magnitude. For an illustration of this technique we refer to figure 2 of Paper I. The technique does require that an excitation temperature be assigned to the CO. The accuracy with which the excitation temperature can be found naturally depends on the number of usable lines. Typically, the excitation temperature could be constrained to better than  $\pm 150$  K. Fortunately, the isotopic ratio is not highly sensitive to the excitation temperature and uncertainties in the  $\pm 150$  range have only a small effect on the resulting isotopic ratios.

To reduce the uncertainty in the abundances in the case of ill-defined excitation temperatures, we investigated the relation between the excitation temperature,  $T_{\text{exc}}$ , and the effective temperature,  $T_{\text{eff}}$ . There is considerable basis for assuming these quantities are related via the atmospheric structure and elemental abundances. Effective temperature is a measure of the total energy integrated over all wavelengths radiated from a unit of stellar surface area. The value is fixed by luminosity and radius and is an observable quantity.  $T_{\text{eff}}$ , is given by the relation

$$F = \left(\frac{\phi}{2}\right)^2 \sigma T_{\text{eff}}^4 \quad (1)$$

where  $F$  is the bolometric flux received at the Earth,  $\sigma$  is the Stefan-Boltzmann constant, and  $\phi$  is the angular diameter (Ridgway et al. 1980). Most values of  $T_{\text{eff}}$  for cool giants have been set using equation 1 with  $\phi$  determined by lunar occultations and interferometry (see, for instance, Ridgway et al. 1980; Richichi et al. 1999) and  $F$  determined from near-IR photometry. Observational limits associated with the techniques restrict the sample of objects both in magnitude, diameter, and position on the sky. A second approach based on infrared flux (Blackwell & Shallis 1977; Blackwell et al. 1990) also produces effective temperatures. Both techniques produce similar results. We limit our discussion to the angular diameter approach.

Effective temperature is known to vary with spectral type, for the M giants nearly linearly (Richichi et al. 1999). Worthey & Lee (2011) present a comparison of  $T_{\text{eff}}$  versus  $V - K$  relations for cool giants. The Bessell et al. (1998)  $T_{\text{eff}}$  versus  $V - K$  relation, derived from a compilation of occultation and interferometry diameters, is the best fit to the Worthey & Lee (2011) data. Sharma et al. (2016) review a number of fits to the  $T_{\text{eff}}$  versus M giant spectral type relation against several groups of synthetic spectra. A  $T_{\text{eff}} - (V - K)$  relation derived from a homogeneous set of angular diameters by Richichi et al. (1999) gives the best match and extends to the coolest non-Mira M giants. Therefore, we adopted the spectral type - effective temperature relation by Richichi et al. (1999) for our study. However, use of the Bessell et al. (1998) calibration would result in negligible change. All the calibrations show scatter around a mean relation. The Richichi et al. (1999) relation shows considerable scatter to lower temperatures.

Since the sample stars are bright, in fact most (Table 1) are in the Yale Bright Star Catalog (Hoffleit 1964), there are well-determined spectral types and magnitudes. We ignore the galactic reddening of these nearby objects. Table 2 lists the parameters for the program stars, including the effective temperatures derived using the Richichi et al. (1999) relation for the M giants. Smith & Lambert (1990) find that S stars of temperature subclass 5 and earlier follow the same effective temperature versus  $V - K$  temperature subclass relation as for the M giants. Following from this, we

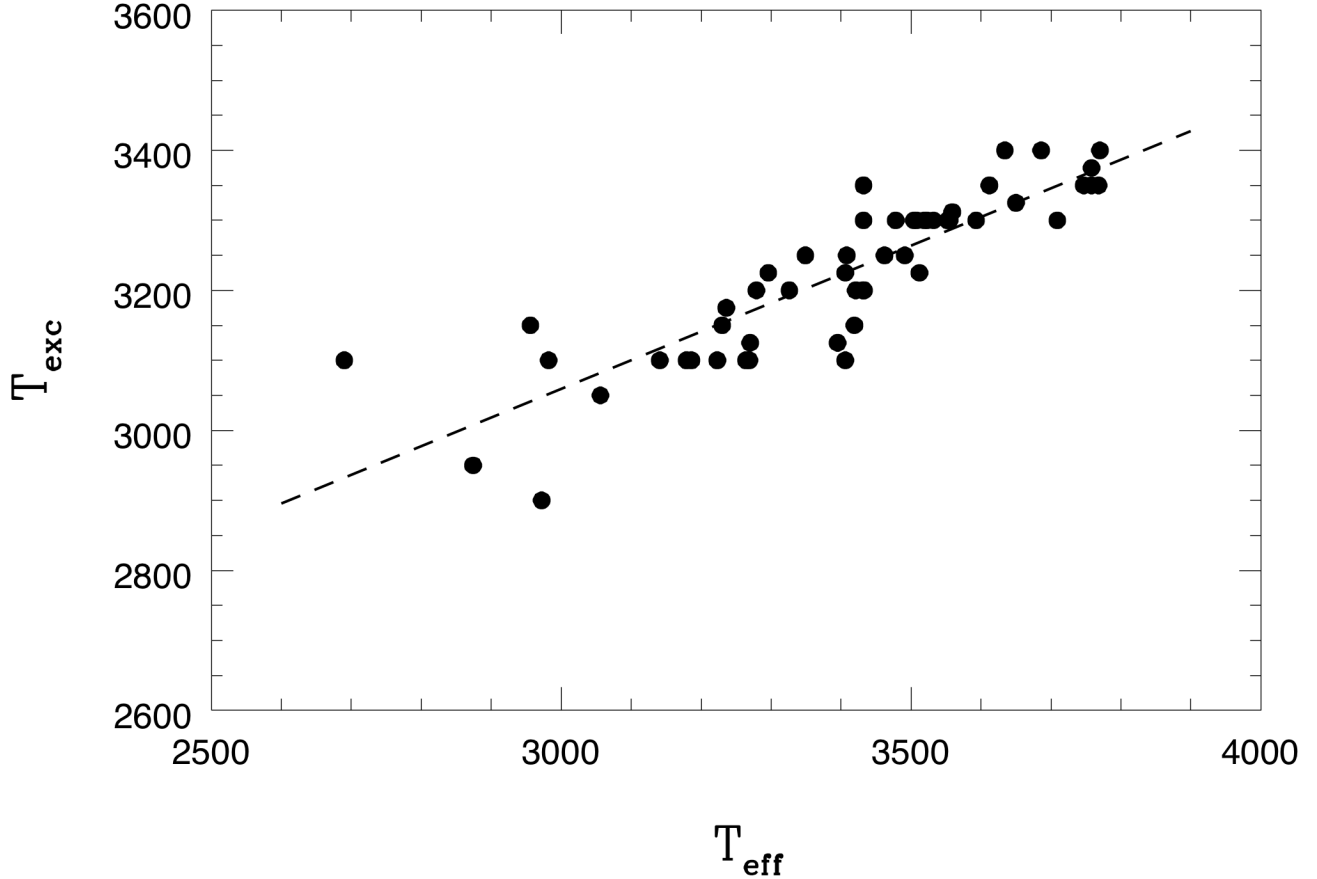


**Figure 1.** Excitation temperatures of the CO second-overtone lines plotted as a function of effective temperature. The effective temperatures for our M- and S-type stars are from V-K colors following [Richichi et al. \(1999\)](#). Dashed line is a fit to the M and S relation.

have assigned effective temperatures for the six S stars earlier than S5 in our data set by using the [Richichi et al. \(1999\)](#) scale. One star, DY Gem, is later than S5. We assume, as did [Smith & Lambert \(1990\)](#), that the effective temperature of this star is the same as an M giant of the same subclass.

Using the method described in Paper I and in [Hinkle et al. \(1976\)](#), we found empirical CO second-overtone excitation temperatures for the sample stars. The resulting excitation temperatures are listed in Table 2 and plotted as a function of effective temperature in Figure 1. A linear least-squares fit gives

$$T_{exc} = 0.4091 T_{eff} + 1832. \quad (2)$$

[Tsuji \(1991\)](#) previously noted the relation between CO second-overtone excitation temperature and effective temperature.

**Table 2.** Effective and excitation temperatures and luminosities for our sample stars

HD/BD	Spec.	V	K	V-K <sup>a</sup>	Date	T <sub>eff</sub>	T <sub>exc</sub>	T <sub>exc</sub>	T <sub>exc</sub>	log (L/L <sub>⊙</sub> )	D <sup>b</sup>
	Type <sup>a</sup>					K	(est.) K	(fit) K	(est.-fit)		pc
HD 6860	M0III	2.05	-1.87	3.92	76 Jun 6	3770	3400	3374	26	...	...

Table 2 continued on next page

Table 2 (continued)

HD/BD	Spec. Type <sup>a</sup>	V	K	V-K <sup>a</sup>	Date	T <sub>eff</sub> K	T <sub>exc</sub> (est.) K	T <sub>exc</sub> (fit) K	T <sub>exc</sub> (est.-fit)	log (L/L <sub>⊙</sub> )	D <sup>b</sup> pc
HD 6860	M0III				79 Jun 14+15		3400				
HD 7351	S3+/2-	6.38	1.64	4.74	77 Jun 29	3532	3300	3277	23	3.132	282 <sup>-14</sup> <sub>+16</sub>
HD 18191	M6III	5.93	-1.02	6.95	76 Aug 17	3236	3175	3156	19	3.178	98 <sup>-5</sup> <sub>+6</sub>
HD 18884	M1.5IIIa	2.53	-1.67	4.20	76 Sep 28	3686	3400	3340	60	...	...
HD 20720	M3/4III	3.70	-1.15	4.85	76 Sep 29	3508	3300	3267	33	3.307	106 <sup>-6</sup> <sub>+7</sub>
HD 22649	S3.5/2	5.11	0.10	5.01	76 May 14	3478	3300	3255	45	3.363	182 <sup>-9</sup> <sub>+10</sub>
HD 30959	M3SIII	4.75	-0.66	5.41	76 Aug 23	3421	3200	3232	-32	3.427	163 <sup>-11</sup> <sub>+12</sub>
HD 30959	M3SIII				78 Jan 22		3200				
HD 39225	M1.5II-III	6.07	1.94	4.13	89 Sep 14	3709	3300	3349	-49	2.736	190 <sup>-6</sup> <sub>+7</sub>
HD 44478	M3IIIab	2.87	-1.49	4.36	76 Sep 29	3634	3400	3319	81	...	...
HD 44478	M3IIIab				79 Sep 5+7+9		3300				
HD 49368	S3/2	7.78	2.46	5.32	87 Apr 14	3432	3350	3236	114	3.501	754 <sup>-23</sup> <sub>+25</sub>
HD 55966	M4IIIa	4.96	-0.15	5.11	90 Apr 12	3462	3250	3248	2	3.256	154 <sup>-5</sup> <sub>+5</sub>
HD 58521	M6S	6.98	-0.44	7.42	78 Jan 22	3179	3100	3133	-33	...	...
HD 64332	S4.5/2	7.64	2.31	5.33	87 Apr 13	3431	3200	3236	-36	3.541	627 <sup>-27</sup> <sub>+30</sub>
HD 71250	M3III	5.50	0.56	4.94	78 Oct 15	3491	3250	3260	-10	3.576	303 <sup>-28</sup> <sub>+34</sub>
HD 94705	M5.5III	5.78	-0.81	6.59	90 Apr 11	3279	3200	3174	26	3.170	106 <sup>-5</sup> <sub>+6</sub>
HD 96360	M3[Swk]	8.09	2.77	5.32	87 Apr 14	3432	3300	3236	64	2.868	417 <sup>-7</sup> <sub>+7</sub>
HD 100029	M0III-IIIa	3.85	-0.12	3.97	90 Apr 12	3758	3375	3369	6	3.139	119 <sup>-6</sup> <sub>+7</sub>
HD 102212	M1III	4.04	0.07	3.97	82 Apr 8	3758	3350	3369	-19	2.915	100 <sup>-6</sup> <sub>+7</sub>
HD 106198	M4/5(I/II)	6.47	-0.24	6.71	87 Apr 13	3264	3100	3167	-67	3.907	431 <sup>-46</sup> <sub>+59</sub>
HD 112300	M2III	3.38	-1.24	4.62	76 Jun 18	3559	3312	3288	24	...	...
HD 112300	M2III				77 Jun 24		3300				
HD 114961	M7 III	6.85	-1.79	8.64	76 Jun 18	3056	3050	3082	-32	4.506	316 <sup>-61</sup> <sub>+100</sub>
HD 119228	M2III	4.66	0.35	4.31	90 Apr 11	3650	3325	3325	0	3.237	168 <sup>-8</sup> <sub>+8</sub>
HD 121130	M3III	4.66	-0.17	4.83	77 Jun 28	3512	3225	3269	-44	3.115	122 <sup>-4</sup> <sub>+4</sub>
HD 123657	M4.5 III	5.28	-0.37	5.65	76 Aug 18	3395	3125	3221	-96	3.537	190 <sup>-12</sup> <sub>+14</sub>
HD 126327	M7-8IIIe	8.60	-1.96	10.56	76 Jan 14	2874	2950	3008	-58	3.633	128 <sup>-5</sup> <sub>+5</sub>
HD 132813	M5III	4.54	-1.00	5.54	76 Aug 18	3406	3100	3225	-125	3.176	100 <sup>-6</sup> <sub>+7</sub>
HD 133216	M3/4III	3.21	-1.43	4.64	76 Aug 18	3555	3300	3286	14	3.587	128 <sup>-12</sup> <sub>+15</sub>
HD 146051	M0.5III	2.75	-1.26	4.01	77 Jun 24	3747	3350	3365	-15	...	...
HD 148783	M6-III	5.01	-2.05	7.06	77 Jun 30	3223	3100	3151	-51	3.696	122 <sup>-5</sup> <sub>+6</sub>
HD 149683	M7III:e	9.44	-0.04	9.48	83 Sep 13	2982	3100	3052	48	3.786	384 <sup>-16</sup> <sub>+18</sub>
HD 154143	M3III	4.98	0.49	4.49	90 Apr 12	3593	3300	3302	-2	2.913	126 <sup>-3</sup> <sub>+3</sub>
HD 163990	M6S	6.32	0.07	6.25	76 Sep 29	3326	3200	3193	7	3.676	275 <sup>-13</sup> <sub>+15</sub>
HD 168574	M3III	6.25	-0.21	6.46	76 Sep 29	3296	3225	3180	45	3.825	322 <sup>-23</sup> <sub>+26</sub>
HD 175588	M4II	4.30	-1.22	5.52	76 Apr 11	3408	3250	3226	24	...	...
HD 175865	M5III	4.00	-2.08	6.08	90 Apr 11	3349	3250	3202	48	2.509	96 <sup>-5</sup> <sub>+6</sub>
HD 182917	M7IIIab	7.08	-0.70	7.78	79 Feb 8	3141	3100	3117	-17	3.302	183 <sup>-7</sup> <sub>+8</sub>
HD 183439	M0III	4.45	0.52	3.93	76 May 16	3768	3350	3374	-24	2.744	100 <sup>-3</sup> <sub>+3</sub>
HD 184313	M5-5.5III	6.48	-0.18	6.66	84 Feb 21	3270	3125	3170	-45	3.508	218 <sup>-10</sup> <sub>+11</sub>
HD 184313	M5-5.5III				84 Nov 13		3100				
HD 196610	M6III	5.89	-1.11	7.00	90 Apr 12	3230	3150	3153	-3	3.291	110 <sup>-4</sup> <sub>+4</sub>
HD 198026	M3III	4.44	-0.21	4.65	76 May 16	3552	3300	3285	15	3.161	126 <sup>-5</sup> <sub>+6</sub>
HD 198164	SC2/7.5	11.00	2.18	8.82	76 Jun 19	2690	3100	2933	167	4.213	1509 <sup>-77</sup> <sub>+86</sub>

Table 2 continued on next page



Table 2 (continued)

HD/BD	Spec. Type <sup>a</sup>	V	K	V-K <sup>a</sup>	Date	$T_{\text{eff}}$ K	$T_{\text{exc}}$ (est.) K	$T_{\text{exc}}$ (fit) K	$T_{\text{exc}}$ (est.-fit)	log (L/L <sub>⊙</sub> )	D <sup>b</sup> pc
HD 200527	M3Ib-II	6.23	0.92	5.31	87 Apr 13	3433	3200	3237	-37	3.674	391 <sup>-21</sup> <sub>+24</sub>
HD 202369	M2III	5.34	0.56	4.78	76 May 12	3523	3300	3273	27	3.156	173 <sup>-9</sup> <sub>+10</sub>
HD 205730	M4e-6eIII	5.38	-1.29	6.67	77 Apr 4	3269	3100	3169	-69	...	...
HD 205730	M4e-6eIII				84 Apr 8		3000				
HD 209872	M7	9.20	-0.55	9.75	83 May 21	2956	3150	3041	109	...	...
HD 209872	M7				84 Nov 13		3150				
HD 216386	M1.2III	3.79	-0.64	4.43	76 Jun 6	3612	3350	3310	40	3.090	94 <sup>-5</sup> <sub>+5</sub>
HD 216672	S4+/1+	6.36	0.94	5.42	77 Jun 4	3419	3150	3231	-81	3.943	422 <sup>-28</sup> <sub>+32</sub>
HD 216672	S4+/1+				88 Jul 2		3200				
HD 217906	M2.5II-III	2.42	-2.38	4.80	76 May 12	3519	3300	3272	28	...	...
HD 218634	M4S	5.14	-0.40	5.54	77 Jun 4	3406	3225	3225	0	3.719	219 <sup>-22</sup> <sub>+27</sub>
HD 224935	M2III	4.41	-0.46	4.87	76 Jun 18	3504	3300	3266	34	3.255	127 <sup>-7</sup> <sub>+8</sub>
HD 260297	S8,5	11.20	1.62	9.58	87 Apr 14	2972	2900	3048	-148	...	...
BD+48 1187	S5/6	9.32	1.96	7.36	77 Aug 25	3186	3100	3135	-35	4.064	616 <sup>-41</sup> <sub>+48</sub>

<sup>a</sup>Spectral type, V, K from Simbad.

<sup>b</sup>Gaia distances and uncertainties from Bailer-Jones et al. (2018)

### 3.2. Surface Gravity

For curve-of-growth analysis only the excitation temperature is required. However, since the stars in the sample have only small velocity amplitudes, it seemed reasonable to explore deriving abundances using spectrum synthesis. This requires the use of a stellar model atmosphere where the inputs include surface gravity. To determine the surface gravity we extracted the distances and brightnesses of the sample stars from Bailer-Jones et al. (2018) based on the Gaia DR2 catalog (Gaia Collaboration et al. 2018). We were able to attribute distances to 40 of the 51 stars in the sample. With these distances we derived luminosities with the help of the mean Gaia G, BP, and RP magnitudes and bolometric corrections given in Lebzelter et al. (2019) which are based on a library of reference objects from Kerschbaum et al. (2010). Limitations in the astrometric solution provided in Gaia DR2<sup>1</sup> could affect the luminosity values used here. Using the luminosity and effective temperature from equation 2 the radius follows from equation 1. As a starting point, we assume a mass of 1.2 M<sub>⊙</sub> for a typical AGB star. These values were in turn used to select model atmospheres from a grid of atmospheres (see Section 4.3. The grid is set in steps of log g. Since the entire range of AGB masses covers less than 1 in the log, the assumed value of 1.2 M<sub>⊙</sub> does not have a large impact on the model atmosphere selected.

## 4. ABUNDANCES

### 4.1. Isotopic ratios of Carbon and Oxygen

Isotopic ratios were determined using the technique described in Paper I. The technique compares weak lines of equal strengths from different isotopes. The isotopic ratio is the shift in the abscissa between the curve of growth for the <sup>12</sup>C<sup>16</sup>O lines and the curve of growth for the rarer isotope. The LTE line strength is plotted on the abscissa, and the reduced equivalent width (equivalent width divided by the wavenumber of the transition) is plotted on the ordinate. References to the input data on the transitions used in our analysis can be found in Paper I.

As in Paper I, the set of lines was selected by searching each vibration-rotation transition that falls in the *H* and *K* bands. For <sup>12</sup>C<sup>17</sup>O, and <sup>12</sup>C<sup>18</sup>O the selection is limited to lines from only 2-0 and 3-1. The <sup>12</sup>C<sup>17</sup>O 2-0 lines from R20 to R33 are well placed (see figure 6 of Wallace & Hinkle 1996) and unless the ratio <sup>16</sup>O/<sup>17</sup>O ratio is very large, lines can be found. On the other hand, the <sup>12</sup>C<sup>18</sup>O lines are mixed in with other CO lines. Nonetheless, a few fairly convincing lines were typically found in each spectrum. A list of lines that show little blending is given in Paper I. For

<sup>1</sup> <https://www.cosmos.esa.int/web/gaia/dr2>

$^{12}\text{C}^{16}\text{O}$  and  $^{13}\text{C}^{16}\text{O}$  lines from the various first- and second-overtone bands were used. Central depths were measured for these lines and transferred into reduced equivalent width.

For all the program stars lines were measured in both the first ( $\Delta v=2$ ) and second ( $\Delta v=3$ )  $^{12}\text{C}^{16}\text{O}$  overtones. For  $^{13}\text{C}^{16}\text{O}$  lines were always present from the first overtone and for cooler stars from both overtones. The two overtones were combined into a single curve of growth for each isotope. The shifts between the curves of growth of the isotopologue give the isotopic ratios. The extreme range of possible shifts is shown by the uncertainties. The resulting isotopic ratios and their uncertainties can be found in Table 3. For some stars we also explored varying the excitation temperature. This was done both to evaluate the dependency of the results on this input parameter and to handle cases where the empirical determination gave a strongly deviating result from the  $T_{\text{exc}} - T_{\text{eff}}$  relation derived in Section 3.1. Paper I demonstrated that the error introduced by typical 100 K uncertainties in the excitation temperature corresponds to errors in the isotopic ratios of C and O of  $\leq 10\%$ .

Where we had more than one spectrum for a star, the differences are typically within the uncertainty limits. Not surprisingly, a lower S/N can prevent the determination of the isotopic ratios of oxygen, for instance in  $\delta$  Vir and W Cyg. The oxygen isotope ratios always compare the  $K$  band first-overtone lines against  $^{12}\text{C}^{16}\text{O}$  second-overtone lines in the  $H$  band. The S/N typically peaks in the middle of the  $K$  band and is about a factor of two lower in the  $H$  band. Since lines of equal strength are compared, in spectra with marginal peak S/N the weak rare oxygen isotopic lines are then compared to weak  $^{12}\text{C}^{16}\text{O}$  dominated by noise. This may also be the cause for the very large difference in  $^{16}\text{O}/^{18}\text{O}$  observed between the two observations of  $\mu$  Gem. Note that the other isotopic ratios for this star are in reasonable agreement. In Paper I we showed that the pulsation phase has very little influence on the measured isotopic ratio. For our sample consisting of small-amplitude variables we expect this effect to be even less relevant.

The shift along the abscissa that gives the isotopic ratio is on a logarithmic scale. When the standard deviation of the shift is then transferred into a linear scale, the resulting error is asymmetric. In some earlier papers, also in our Paper I, a single mean value was given for the error, overestimating the uncertainty on the negative side and underestimating it on the positive side. In the present paper we decided to list the asymmetric error and to use it also in the plots where applicable.

**Table 3.** Measured Values for C and O Isotopes

HD/BD	Var name	$^{12}\text{C}/^{13}\text{C}$		$^{16}\text{O}/^{17}\text{O}$		$^{16}\text{O}/^{18}\text{O}$	
		mean	low/hi	mean	low/hi	mean	low/hi
HD 6860	$\beta$ And 06/76	10	9/11	239	181/316	2199	1825/2649
HD 6860	$\beta$ And 06/79	10	9/12	158	122/204	578	240/1389
HD 7351	DT Psc	16	13/19	>5000	...	...	
HD 18191	RZ Ari	6	5/7	958	491/1870	2422	1626/3607
HD 18884	$\alpha$ Cet	11	6/20	660	532/819	730	590/904
HD 20720	$\tau^4$ Eri	8	7/11	598	189/1891	473	181/1238
HD 22649	BD Cam	14	10/20	486	269/880	140	77/255
HD 30959	$\sigma^1$ Ori 08/76	16	14/21	532	397/713	513	260/1012
HD 30959	$\sigma^1$ Ori 01/78	15	14/19	360	306/424	827	438/561
HD 39225	HR 2028	10	7/13	600	206/1750	977	482/1981
HD 44478	$\mu$ Gem 09/76	11	5/23	618	347/1101	2430	1444/4087
HD 44478	$\mu$ Gem 09/79	10	8/13	660	445/978	409	193/868
HD 49368	V613 Mon	16	13/20	556	333/928	1103	663/1835
HD 55966	VZ Cam	14	11/18	3924	2942/5235	761	514/1126
HD 58521	Y Lyn	39	32/47	1087	479/2465	387	233/643
HD 64332	NQ Pup	20	18/22	534	319/893	1643	744/3628
HD 71250	BP Cnc	9	7/11	3284	1786/6041	2064	1130/3773
HD 94705	VY Leo	8	6/11	2187	1309/3655	2418	1279/4571

**Table 3** continued on next page

**Table 3** (*continued*)

HD/BD	Var name	$^{12}\text{C}/^{13}\text{C}$		$^{16}\text{O}/^{17}\text{O}$		$^{16}\text{O}/^{18}\text{O}$	
		mean	low/hi	mean	low/hi	mean	low/hi
HD 96360	HL UMa	11	8/16	>5000	...	355	202/623
HD 100029	$\lambda$ Dra	9	7/13	1290	705/2361	664	262/1683
HD 102212	$\nu$ Vir	8	6/10	>2300	...	>2300	...
HD 106198	V335 Hya	18	14/20	497	265/934	562	312/1015
HD 112300	$\delta$ Vir 06/76	13	13/14	...	...	...	...
HD 112300	$\delta$ Vir 06/77	18	14/20	>5000	...	928	568/1517
HD 114961	SW Vir	30	22/40	530	173/1623	591	250/1400
HD 119228	IQ UMa	14	13/18	1535	869/2713	657	166/2606
HD 121130	CU Dra	10	8/15	228	177/295	...	...
HD 123657	BY Boo	10	9/13	2056	1586/2666	...	...
HD 126327	RX Boo	16	13/20	301	151/599	247	155/393
HD 132813	RR UMi	15	10/18	>5000	...	656	434/992
HD 133216	$\sigma$ Lib	6	3/10	>2000	...	>2000	...
HD 146051	$\delta$ Oph	11	8/15	1424	895/2268	1322	414/4219
HD 148783	g Her	13	9/17	723	449/1166	853	412/1766
HD 149683	R UMi	14	11/19	1128	426/2982	618	545/702
HD 154143	HR 6337	12	10/15	1836	1097/3071	640	450/911
HD 163990	OP Her	14	10/18	435	230/821	478	244/939
HD 168574	V4028 Sgr	15	13/18	742	486/1134	1319	568/3065
HD 175588	$\delta^2$ Lyr	21	18/25	1035	830/1292	660	397/1098
HD 175865	R Lyr	18	16/21	829	400/1716	523	310/883
HD 182917	CH Cyg	15	12/18	885	490/1595	464	333/648
HD 183439	$\alpha$ Vul	14	10/17	2079	1096/3943	1880	522/6775
HD 184313	V450 Aql 02/84	14	11/17	964	348/2671	329	215/503
HD 184313	V450 Aql 11/84	14	12/17	1970	969/4004	431	210/882
HD 196610	EU Del	17	13/20	>5000	...	1072	593/1939
HD 198026	EN Aqr	10	8/12	...	...	...	...
HD 198164	CY Cyg	7	6/11	94	25/342	...	...
HD 200527	V1981 Cyg	22	19/27	845	420/1699	745	297/1869
HD 202369	29 Cap	12	9/14	1788	1412/2266	...	...
HD 205730	W Cyg 04/77	13	11/17	1448	964/2174	...	...
HD 205730	W Cyg 08/84	15	12/20	1713	905/3245	515	230/1154
HD 209872	SV Peg 05/83	20	17/23	168	12/2353	345	285/418
HD 209872	SV Peg 11/84	17	14/21	314	191/516	341	210/554
HD 216386	$\lambda$ Aqr	9	4/15	4003	3748/4276	3167	1923/5215
HD 216672	HR Peg 06/76	22	18/28	737	492/1105	223	153/325
HD 216672	HR Peg 06/77	14	6/32	1800:	...	2386	2106/2705
HD 217906	$\beta$ Peg	9	8/10	>5000	...	827	587/1163
HD 218634	GZ Peg	11	10/12	169	54/532	86	43/171
HD 224935	YY Psc	11	10/12	648	348/1205	450	243/833
HD 260297	DY Gem	56	40/79	733	285/1885	704	395/1257
BD+48 1187	TV Aur 08/77	29	26/32	213	82/552	149	68/325
BD+48 1187	TV Aur 04/87	52	43/63	237	194/291	342	315/371

4.2. *Comparison with literature values*

Various of the C and O isotope ratios for a number of the stars in the sample have previously been reported in the literature (Table 4). Some of these results are based on the same spectra used here. References are given at the end

of the table. In some cases, the literature values for the same star, but not necessarily from the same data material, deviate significantly from each other. For a comparison of previously determined values with our results (Figs. 2 and 3) we averaged the isotopic ratios from the literature if they showed the same order of magnitude. In the case values deviating more strongly, computing such an average would not have much value, and we decided to include the ratio closer to our result in the comparison. Of course, this includes the risk of reinforcing a wrong result.

**Table 4.** Literature Values for C and O Isotopes

HD/BD	Var	Lit $^{12}\text{C}/^{13}\text{C}$	Lit $^{16}\text{O}/^{17}\text{O}$	Lit $^{16}\text{O}/^{18}\text{O}$
	Name	ref (value)	ref (value)	ref (value)
HD 6860	$\beta$ And	1 (10), 4 (11 $\pm$ 3)	13 (170 $\pm$ 10)	13 (425 $_{+150}^{-75}$ )
HD 7351	DT Psc	4 (12 $\pm$ 4), 12 (24 $_{+16}^{-8}$ )	12 (3000 $_{+2500}^{-1200}$ ), 4 (2500)	4 (2250), 12 (4600 $_{+5900}^{-2100}$ ) <sup>(1)</sup>
HD 18191	RZ Ari	1 (10), 11 (7.9 $\pm$ 0.8)	11 (607 $\pm$ 48)	...
HD 18884	$\alpha$ Cet	1 (10), 11 (11.1 $\pm$ 0.8)	11 (586 $\pm$ 47)	...
HD 20720	$\tau^4$ Eri	11 (12.4 $\pm$ 0.3)	11 (687 $\pm$ 14)	...
HD 22649	BD Cam	2 (34), 4 (25 $\pm$ 4), 12 (55 $_{+32}^{-18}$ )	4 (350), 12 (2250 $_{+700}^{-550}$ )	12 (4700 $_{+2200}^{-1400}$ ), 4 (650)
HD 30959	$\text{o}^1$ Ori	1 (10), 4 (18 $\pm$ 2), 12 (25 $_{+12}^{-6}$ )	4 (480), 12 (925 $_{+270}^{-225}$ )	4 (640), 12 (1350 $_{+850}^{-450}$ )
HD 39225	HR 2028	3 (9 $\pm$ 1.4)	3 (>260)	...
HD 44478	$\mu$ Gem	2 (15), 4 (13 $\pm$ 2), 11 (10.5 $\pm$ 1.2)	11 (798 $\pm$ 73), 13 (325 $_{+150}^{-75}$ )	13 (475 $_{+200}^{-125}$ )
HD 49368	V613 Mon	4 (14 $\pm$ 2)	4 (430)	4 (>800)
HD 58521	Y Lyn	4 (43 $\pm$ 8), 10 (27)	4 (560)	4 (630)
HD 64332	NQ Pup	4 (18 $\pm$ 4)	4 (400)	4 (720)
HD 96360	HL UMa	4 (13 $\pm$ 2)	4 (1900)	4 (450)
HD 100029	$\lambda$ Dra	3 (7 $\pm$ 1.7)	3 (>85)	...
HD 102212	$\nu$ Vir	4 (12 $\pm$ 2), 11 (8.7 $\pm$ 1.3)	11 (>2000)	...
HD 106198	V335 Hya	4 (19 $\pm$ 5)	4 (350)	4 (1120)
HD 112300	$\delta$ Vir	4 (16 $\pm$ 4), 11 (12.3 $\pm$ 1.2)	11 (>2500)	...
HD 114961	SW Vir	10 (18), 11 (22.0 $\pm$ 4.7)	11 (432 $\pm$ 37)	...
HD 121130	CU Dra	2 (10), 4 (12 $\pm$ 3), 11 (14.8 $\pm$ 1.6)	11 (151 $\pm$ 11)	...
HD 123657	BY Boo	4 (9 $\pm$ 2)	...	...
HD 126327	RX Boo	9 (17)	11 (233 $\pm$ 20)	...
HD 132813	RR UMi	11 (10.0 $\pm$ 0.8)	11 (>2000)	...
HD 133216	$\sigma$ Lib	11 (7.5 $\pm$ 0.3)	11 (>1500)	...
HD 146051	$\delta$ Oph	1 (30), 11 (11.1 $\pm$ 0.9)	11 (387 $\pm$ 68)	...
HD 148783	g Her	4 (10 $\pm$ 2), 13 (12.5 $\pm$ 1.1), 12 (16 $_{+9}^{-6}$ )	11 (211 $\pm$ 42), 14 (675 $\pm$ 175)	12 (850 $_{+500}^{-300}$ )
HD 149683	R UMi	10 (15 $\pm$ 3)	10 (1862 $\pm$ 700)	10 (525 $\pm$ 120)
HD 163990	OP Her	4 (20 $\pm$ 2), 13 (11.3 $\pm$ 1.2), 12 (21 $_{+14}^{-7}$ )	4 (360), 11 (329 $\pm$ 31), 12 (850 $_{+275}^{-200}$ )	4 (590) 12 (1200 $_{+525}^{-350}$ )
HD 168574	V4028 Sgr	11 (48.5 $\pm$ 2.9)	11 (>1000)	...
HD 175588	$\delta^2$ Lyr	1 (10), 11 (16.2 $\pm$ 1.5)	11 (465 $\pm$ 41)	...
HD 175865	R Lyr	11 (6.4 $\pm$ 0.3)	11 (368 $\pm$ 44)	...
HD 182917	CH Cyg	14 (18 $_{-6}^{+12}$ )	14 (830 $_{-270}^{+400}$ )	14 (>1000)
HD 183439	$\alpha$ Vul	1 (10), 4 (7 $\pm$ 3)	...	...
HD 198026	EN Aqr	1 (10)	...	...
HD 198164	CY Cyg	15 (5.6 $\pm$ 1.2), 18 (5)	15 (350 $\pm$ 120), 19 (620 $\pm$ 50)	16 (770 $\pm$ 500)
HD 200527	V1981 Cyg	2 (46), 4 (23 $\pm$ 5),	4 (550), 12 (1850 $_{+550}^{-425}$ )	4 (>1300), 12 (3200 $_{+1250}^{-900}$ )

**Table 4** continued on next page

Table 4 (continued)

HD/BD	Var	Lit $^{12}\text{C}/^{13}\text{C}$	Lit $^{16}\text{O}/^{17}\text{O}$	Lit $^{16}\text{O}/^{18}\text{O}$
	Name	ref (value)	ref (value)	ref (value)
		12 ( $39_{-20}^{-12}$ )		
HD 216386	$\lambda$ Aqr	1 (3), 11 ( $7.9\pm 1.4$ )	11 (>1000)	...
HD 216672	HR Peg	2 (63), 12 ( $71_{+34}^{-21}$ )	12 ( $2400_{+850}^{-600}$ )	12 ( $3000_{+2000}^{-1100}$ )
HD 217906	$\beta$ Peg	1 (10), 4 ( $8\pm 2$ ), 11 ( $7.7\pm 0.5$ )	11 (>2500), 13 ( $1050_{+500}^{-250}$ )	13 ( $425_{+150}^{-75}$ )
HD 218634	GZ Peg	1 (30)	...	...
HD 224935	YY Psc	1 (10)	...	...
HD 260297	DY Gem	4 ( $30\pm 7$ )	4 (570)	4 (1210)
BD+48 1187	TV Aur	4 ( $5\pm 2$ )	4 (240)	4 (440)

NOTE—Note that the references cover the period from 1985 to later. 1=Lazaro et al. (1991) models only have 12/13 = 3, 10, 30, 60; 2=Smith & Lambert (1986); 3=Wallerstein & Morell (1994); 4=Smith & Lambert (1990) see Smith and Lambert 1985 ApJ 294 326 for stellar parameters; 5=Lambert et al. (1986)  $^{12}\text{C}/^{13}\text{C}$  from table 4, uncertainties rough average of table 6, spectra same as ours; 6=Ohnaka & Tsuji (1996); 7=Harris et al. (1987); 8=Schöier & Olofsson (2000); 9=Ramstedt & Olofsson (2014); 10=Hinkle et al. (2016); 11=Tsuji (2008); 12=Harris et al. (1985); 13=Harris & Lambert (1984b); 14=Schmidt et al. (2006); 15=Dominy et al. (1986); 16=Abia et al. (2017), spectra same as ours.

It can be seen from Figure 2 that for the carbon isotopic ratio the majority of our results are in reasonable agreement with the literature results considering the uncertainties. We note that on average our values tend to be slightly lower than the results in the literature. However, there are a few stars with strongly deviating  $^{12}\text{C}/^{13}\text{C}$  given in the literature, even though some results have been deduced from the spectra we used in our analysis.

#### 4.2.1. Discrepant $^{12}\text{C}/^{13}\text{C}$ Cases

HR Peg has been studied by Smith & Lambert (1986) who found  $^{12}\text{C}/^{13}\text{C} = 63$ , while our value is 22. A similar case, with the same literature reference, is BD Cam, for which we found  $^{12}\text{C}/^{13}\text{C} = 14$  while Smith & Lambert (1986) report a ratio of 34, later refined to 25 (Smith & Lambert 1990). To make this more puzzling, the same archival FTS spectra were used in both analyses. The spectra have the problem of poor overlap between the  $^{12}\text{CO}$  and  $^{13}\text{CO}$  curves of growth. The  $^{13}\text{CO}$  second-overtone lines have depths of only a few percent of the continuum, and at a S/N around 50 in the  $H$ -band the noise is of similar size. The S stars do have strong CO, and saturation is a problem for the first overtone.

To explore this further a synthetic  $H$ -band spectrum was computed for HR Peg for different  $^{12}\text{C}/^{13}\text{C}$  ratios. In Figure 4 we compare the observed spectrum with the models showing the  $H$ -band region also used by Smith & Lambert (1986). The two  $^{13}\text{CO}$  lines visible in this figure show a divergent result. The 5-2 R48 line, used, among others, by Smith & Lambert, is strongly affected by the neighboring OH line, but the depth indeed suggests a  $^{12}\text{C}/^{13}\text{C}$  ratio of more than 25. On the other hand, the 5-2 R22 line strongly favors a lower ratio. The plot clearly shows the weakness of the second-overtone lines and the according difficulty in determining the correct value. The problem appears to be the marginal usefulness of the observed spectrum. A high-S/N spectrum in the  $H$ -band would settle this discrepancy.

The literature value for  $^{12}\text{C}/^{13}\text{C}$  in V4028 Sgr (Tsuji 2008) is 48. As was the case for HR Peg and BD Cam the same FTS spectrum has been used in both studies. However, the methods are different, with Tsuji's analysis being based on one single line. Tsuji notes that the uncertainty can be much larger in this case than the formal error, which is reproduced in Table 4. A comparison between observed and a synthetic spectrum with  $T_{\text{eff}}=3300\text{K}$  and  $\log g=0.0$  supports our  $^{12}\text{C}/^{13}\text{C} \sim 15$ . In the course of the modeling, the oxygen isotopic ratios of V4028 Sgr were confirmed within the error bars, with the synthetic spectra comparison favoring a slightly higher  $^{16}\text{O}/^{17}\text{O}$  value.

TV Aur has a literature value of  $^{12}\text{C}/^{13}\text{C} = 5\pm 2$  reported by Smith & Lambert (1990). The star was observed twice with the FTS, once in 1977 and again in 1987 (Table 1). We have analyzed both spectra and assume the Smith & Lambert (1990) result is based on the second. Both spectra have strong  $^{12}\text{CO}$  lines with the second-overtone lines reaching depths of 75%. By contrast the  $^{13}\text{CO}$  second-overtone lines are only marginally detectable in the spectra. This requires that the  $^{12}\text{C}/^{13}\text{C}$  ratio be large and clearly excludes values  $\lesssim 10$ . The extraordinary strength of the  $^{12}\text{CO}$  second-overtone lines indicates the lines are saturated. The available model atmospheres and spectrum synthesis techniques, such as those employed by Smith & Lambert (1990), are not adequate for this star. The low S/N in the  $H$ -band of both archival FTS spectra limits the accuracy of our results. We confirmed that both FTS spectra were of

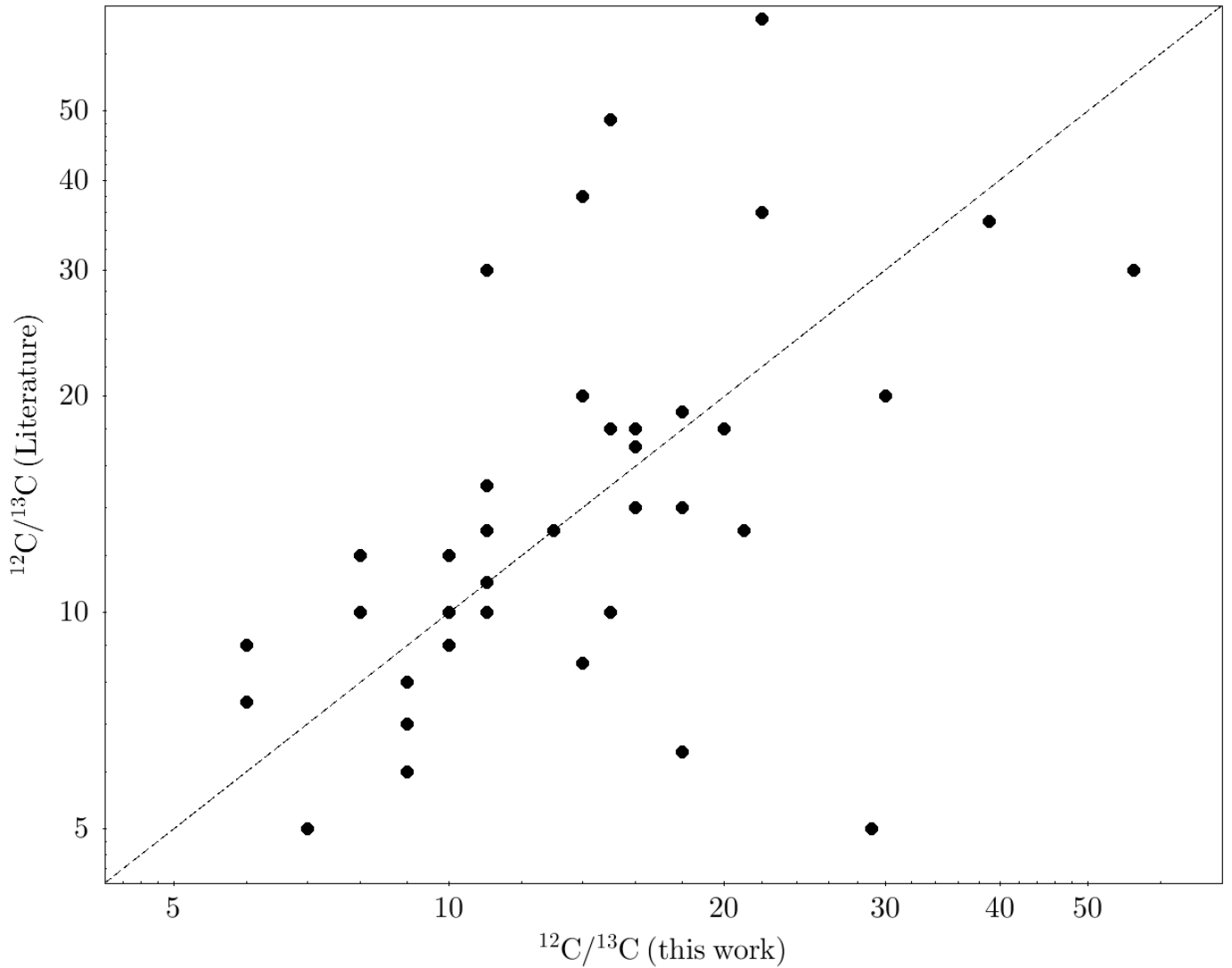


**Figure 2.** Comparison of  $^{12}\text{C}/^{13}\text{C}$  ratios from the literature with our results. The dashed line marks a 1:1 relation.

TV Aur by checking the radial velocity against the Gaia value. The isotopic ratios we derive from both spectra are similar and we adapt the average  $^{12}\text{C}/^{13}\text{C} = 40 \pm 10$ .

#### 4.2.2. Extreme $^{16}\text{O}/^{17}\text{O}$ Values

For the  $^{16}\text{O}/^{17}\text{O}$  (Figure 3) we find good agreement with previous studies confirming the outcome of our analysis. In the case of HR Peg we note that the oxygen isotope values derived from a higher-S/N, higher-resolution spectrum agree with the literature values, while values derived from an inferior spectrum do not. The very large values found for some stars have to be taken with caution since the  $\text{C}^{17}\text{O}$  lines become very weak in these cases and are even at an S/N=100 at the limit of detection. For these very small values, small errors in placing the continuum make large differences in the isotopic ratio. Accordingly, we decided to show only lower limits in Table 3 in these cases. We do not present a plot comparing our result with literature values for the  $^{16}\text{O}/^{18}\text{O}$  because of the small number of literature values available.

#### 4.3. Comparison with synthetic spectra

Due to their large variability amplitudes and the dynamic nature of their atmospheres, the miras discussed in Hinkle et al. (2016) are not suitable for modeling with hydrostatic spectra (Lebzelter et al. 2015b). However, the sample used in this paper consists of stars with comparably mild pulsations. Therefore, we also derive isotopic ratios for oxygen by comparing our FTS spectra with synthetic spectra with a goal of comparing the methods.

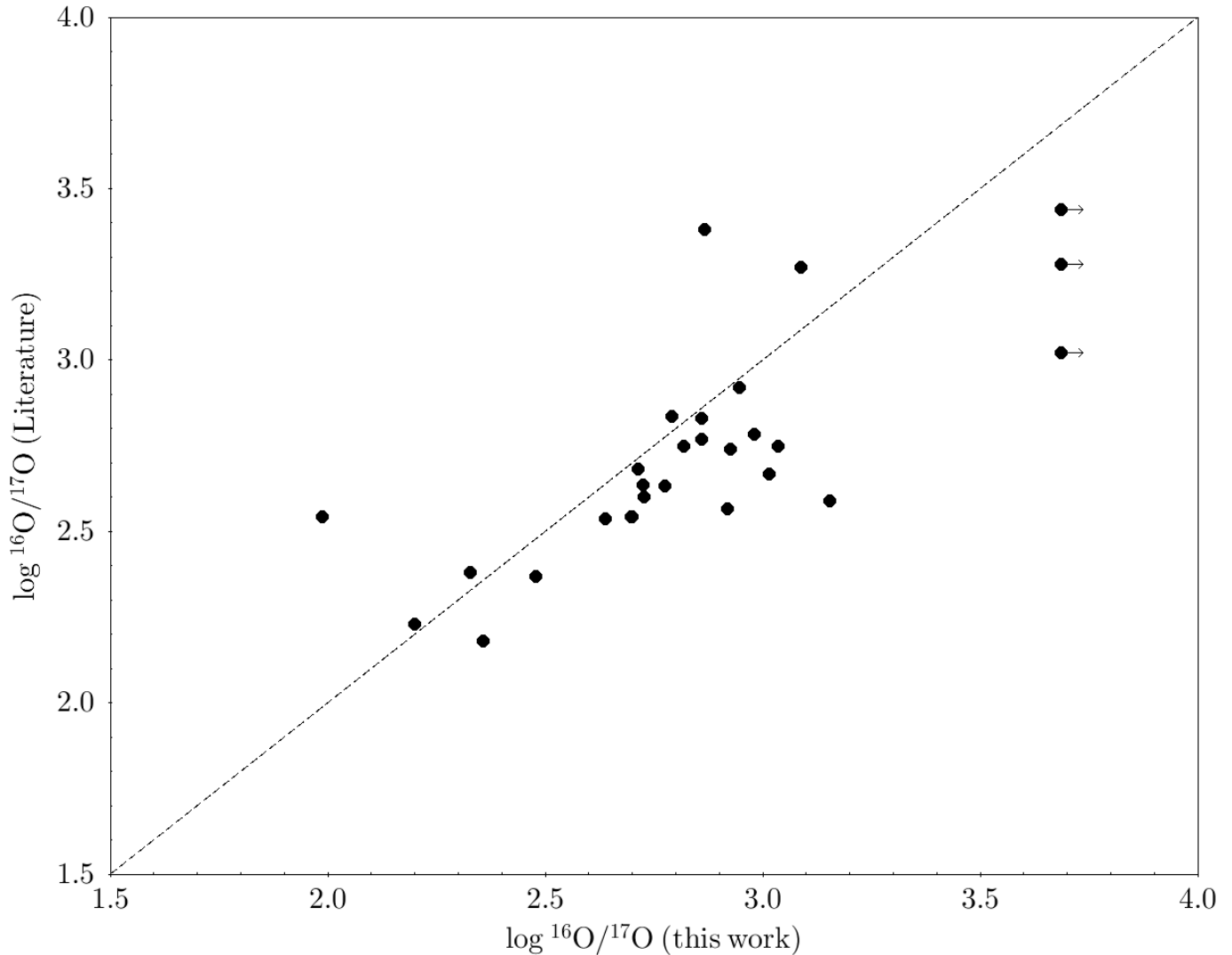


**Figure 3.** Comparison of  $^{16}\text{O}/^{17}\text{O}$  ratios from the literature with our results. The dashed line marks a 1:1 relation. Due to the large range covered by the isotopic ratios of oxygen, a logarithmic scale was used. Data points with arrows denote lower limits.

We used hydrostatic atmospheres from the COMARCS grid of models by Aringer et al. (2016), and computed spectra with the help of the COMA code (Aringer et al. 2016, and references therein). The effective temperatures were taken from the relation between  $T_{\text{exc}}$  and  $T_{\text{eff}}$  derived in Section 3.1. The  $\log g$  values were computed from Gaia data as discussed above. From our sample of SRBs we selected a subset of objects (Table 5) with small uncertainties in the Gaia distances covering a wide range in effective temperature. Preference was given to stars whose parameters were close to the models provided by the COMARCS grid. For all stars we assumed solar metallicity. Since our sample consists exclusively of bright, nearby stars, this assumption seems acceptable. Small deviations from solar metallicity do not affect the outcome of the modelling process significantly. For each of these sets of stellar parameters we computed synthetic spectra for various isotopic ratios of oxygen. The ratios of C/O and  $^{12}\text{C}/^{13}\text{C}$  were set to constant values of 0.3 and 10, respectively. We did some tests to confirm that changing from  $^{12}\text{C}/^{13}\text{C} = 10$  to 25 does not have a visible effect on the spectral regions investigated for the oxygen isotopes, nor do small changes in C/O. The observational data were the telluric corrected spectra. The continua were the same as for the curve-of-growth measurements.

An example of a model fit is shown in Figure 5 for the star HR 4267. Table 5 presents the resulting  $^{16}\text{O}/^{17}\text{O}$  and  $^{16}\text{O}/^{18}\text{O}$  ratios derived from spectral synthesis and compares them with the results from curve-of-growth analysis. The spectrum synthesis approach focused on fitting the  $^{16}\text{O}/^{17}\text{O}$  2-0 R25 to R32 lines and the  $^{16}\text{O}/^{18}\text{O}$  2-0 R23 and R29 lines, respectively. For each line we determined the most appropriate model ratios, and finally averaged over all

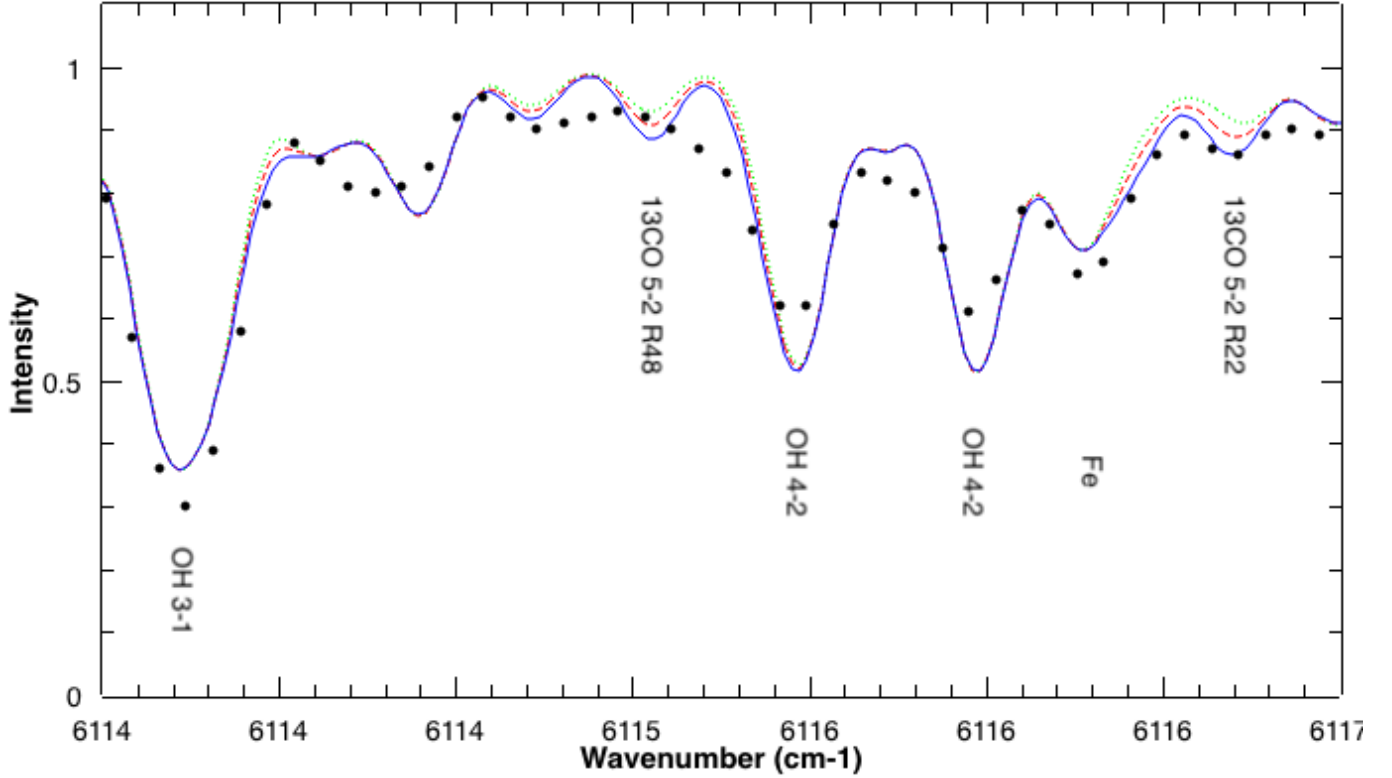


**Figure 4.** FTS spectrum of HR Peg compared with a hydrostatic model atmosphere with  $T_{\text{eff}}=3500\text{K}$  and  $\log g = 1.0$ . The solid (blue), dashed (red) and dotted (green) lines are for  $^{12}\text{C}/^{13}\text{C}$  ratios of 14, 25, and 62, respectively.

**Table 5.** Comparison of the Results between Curve-of-growth Analysis and Spectrum Synthesis Analysis for the Ratios the Oxygen Isotopes.

HD	Var Name	CoG				spectrum synthesis			
		$T_{\text{eff}}$ [K]	$\log g$	$^{16}\text{O}/^{17}\text{O}$	$^{16}\text{O}/^{18}\text{O}$	$T_{\text{eff}}$ [K]	$\log g$	$^{16}\text{O}/^{17}\text{O}$	$^{16}\text{O}/^{18}\text{O}$
HD 18191	RZ Ari	3236	0.36	$900^{+850}_{-400}$	$2200^{+600}_{-400}$	3200	0.5	$1600\pm 300$	$5000\pm 1000$
HD 39225		3709	1.04	$600^{+1100}_{-400}$	$1000^{+900}_{-500}$	3700	1.0	$650\pm 400$	$1300\pm 400$
HD 71250	BP Cnc	3491	0.09	$3300^{+2700}_{-1900}$	$2050^{+1700}_{-900}$	3500	0.0	$3500\pm 1250$	2500:
HD 94705	VY Leo	3279	0.64	$2200^{+1400}_{-900}$	$2400^{+2200}_{-1100}$	3300	0.5	$1900\pm 300$	$2500\pm 500$
HD 100029	$\lambda$ Dra	3758	1.04	$1300^{+1000}_{-600}$	$650^{+1000}_{-400}$	3800	1.0	$1700\pm 400$	$650\pm 70$
HD 126327	RX Boo	2874	-0.30	$300^{+300}_{-150}$	$250^{+150}_{-100}$	2900	-0.5	$1000\pm 200$	$1450\pm 500$
HD 132813	RR UMi	3406	0.53	$>5000$	$550^{+300}_{-200}$	3400	0.5	$1700\pm 450$	$725\pm 100$
HD 133216	$\sigma$ Lib	3555	0.10	$>2000$	$>2000$	3600	0.0	$3700\pm 1400$	$1600\pm 600$
HD 183439	$\alpha$ Vul	3768	1.06	$2100^{+1800}_{-1000}$	$1900^{+4900}_{-1300}$	3800	1.0	$3700\pm 2300$	$1900\pm 200$
HD 184313	V450 Aql	3270	0.05	$1000^{+1700}_{-650}$	$300^{+200}_{-100}$	3300	0.0	$2000\pm 750$	$700\pm 400$

NOTE—For the spectrum synthesis method, columns  $T_{\text{eff}}$  and  $\log g$  give the parameters of the hydrostatic model used.

lines to get the isotopic ratios and uncertainties listed in Table 5. In cases in which one of these lines was obviously blended with a different stellar line or affected by incomplete telluric correction, it was rejected.

We find that for most stars of our subsample the values for the isotopic ratios agree for the two methods within the error bars. It is noteworthy that the error bars of the two methods are quite different in size. Here we have to consider that for the spectrum synthesis we did not include uncertainties in the stellar parameters. The error bars



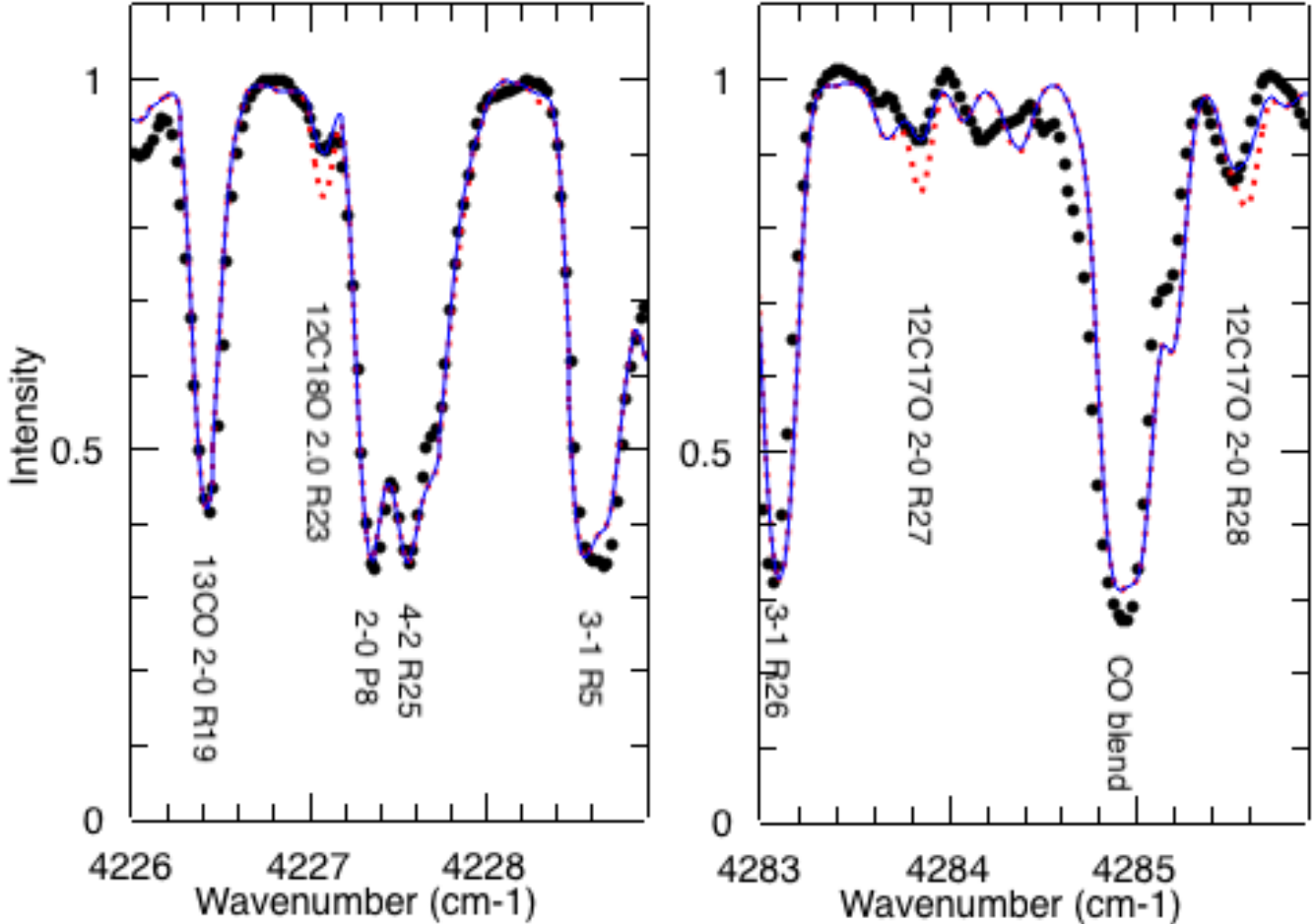


**Figure 5.** Model fit to the FTS spectrum of HR 4267. Big dots: observed spectrum. Left panel: part of the spectrum around the  $^{12}\text{C}^{18}\text{O}$  2-0 R23 line; red dotted line:  $^{16}\text{O}/^{18}\text{O}=1000$ ; blue solid line:  $^{16}\text{O}/^{18}\text{O}=2400$ . Right panel:  $^{12}\text{C}^{17}\text{O}$  2-0 R27 and R28 lines; red dotted line:  $^{16}\text{O}/^{17}\text{O}=1000$ ; blue solid line:  $^{16}\text{O}/^{17}\text{O}=2000$ .

given for the spectrum synthesis method in Table 5 reflect the line-to-line variation only since our comparison of the two approaches aimed at testing their consistency with each other.

Significant differences between the results from the two methods are visible for the stars HR 867, HR 5589, and RX Boo. The first two stars still show values of the same order of magnitude, which is the relevant information for the analysis we attempt in this paper. For RX Boo (Figure 6), however, the two methods lead to different conclusions, in particular in the case of  $^{16}\text{O}/^{18}\text{O}$ . RX Boo is the coolest and most variable star in our subsample, and this finding may indicate a problem occurring for similar objects. The temperature of this star is already at the lower end of our  $T_{\text{exc}} - T_{\text{eff}}$  relation, and it is not clear whether the relation derived is still valid in this temperature regime. RX Boo has a visual light amplitude around 2.5 mag. We have pointed out in Paper I and in Lebzelter et al. (2015b) that with increasing variability the assumption of a hydrostatic atmosphere is no longer appropriate. For consistency and considering the uncertainties of stellar modeling we did not account for in our exemplary study, we use the values derived by the curve-of-growth analysis in the following. Clearly the curve-of-growth analysis has its shortcomings as well; thus, we refrain here from deciding on which method provides the more reliable results. For stars with temperatures above 3000 K and small variability amplitudes, our comparison shows that both methods lead to very similar conclusions. For the cooler M giants the spectrum synthesis technique is increasingly questionable.

For the star HR 5603 the curve-of-growth analysis allowed us to derive lower limits for the two oxygen isotopic ratios only. In this case we will, as an exception, use the values derived from spectrum synthesis in the following analysis.

## 5. DISCUSSION

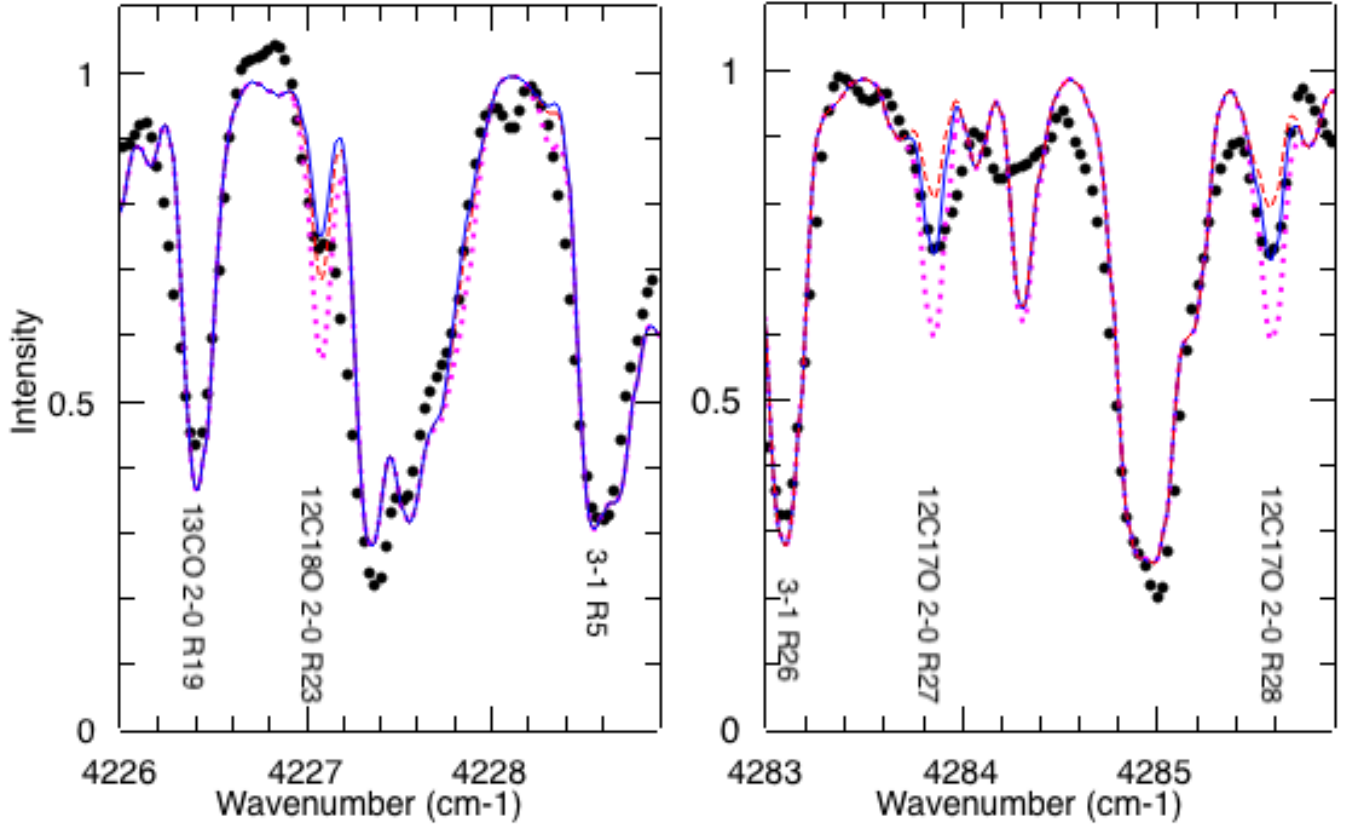


**Figure 6.** Model fit to the FTS spectrum of RX Boo. Big dots: observed spectrum. Left panel: part of the spectrum around the  $^{12}\text{C}^{18}\text{O}$  2-0 R23 line; magenta dotted line:  $^{16}\text{O}/^{18}\text{O}=250$ ; red dashed line:  $^{16}\text{O}/^{18}\text{O}=1000$ ; blue solid line:  $^{16}\text{O}/^{18}\text{O}=2000$ . Right panel:  $^{12}\text{C}^{17}\text{O}$  2-0 R27 and R28 lines; magenta dotted line:  $^{16}\text{O}/^{17}\text{O}=300$ ; blue solid line:  $^{16}\text{O}/^{17}\text{O}=1000$ ; red dashed line:  $^{16}\text{O}/^{17}\text{O}=2000$ .

### 5.1. Mass Estimates for SRb Variables Based on Isotopic Ratios

Throughout the following discussion we assume that our sample consists of single stars. In close binary systems, mass transfer could have changed the isotopic ratios on the surface significantly. The carbon isotopic ratio is low for almost all stars of our sample. The values found are typical for a post-first-dredge-up composition, in many cases likely modified by extra mixing on the RGB to reach values below 10. This suggests that the SRbs studied here are, with a few exceptions, low-mass stars that have not experienced a third dredge-up either because they are still on the RGB/early AGB or because their envelope mass is too low for a third dredge-up to occur.

To confirm the low masses of the sample stars an HRD was constructed (Figure 7) using the values for  $T_{\text{eff}}$  and  $L$  from Section 4. Reddening was not taken into account. A few stars in the sample lack reliable Gaia data and are not included. Figure 7 also includes evolutionary tracks from the FRUITY database (Cristallo et al. 2011) for ZAMS masses of 1.3, 1.5, 2.0 and 2.5  $M_{\odot}$ , respectively. Short time variations during a thermal pulse episode have been omitted for the sake of clarity, since stars are likely observed during the longer interpulse periods. The luminosity depends on the He core mass, which is very similar for the four tracks shown, while the effective temperature is mainly defined by stellar mass and chemical composition (O- or C-rich). Obviously, our sample stars are located in the range spanned by the chosen evolutionary tracks except for a few bright objects.

The figure shows how the sample is divided between early-AGB/bright RGB stars and objects showing thermal pulses (dashed horizontal line). Comparing the stars on the TP-AGB with the evolutionary tracks, we find that most of these objects have likely not experienced a third dredge-up event yet (objects below the red dashed line in Figure 7). Only six stars are clearly above the limit for third dredge-up: SW Vir, CY Cyg, TV Aur, HR Peg, V335 Hya, and V4028 Sgr (ordered by decreasing luminosity). Half are S-type stars which will be discussed in detail in Section 5.2.

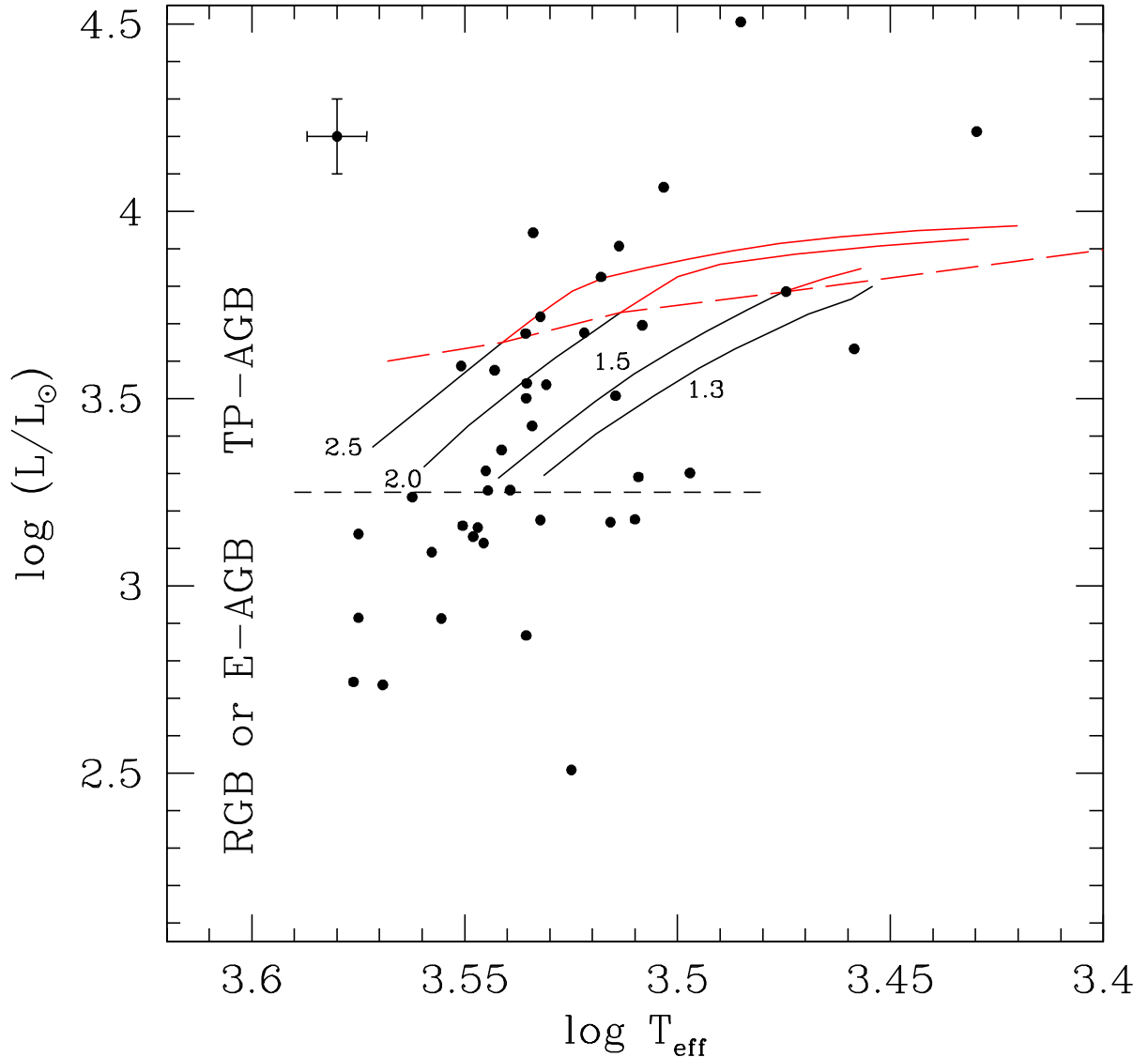


**Figure 7.** Hertzsprung-Russell-Diagram for our sample stars. Overplotted are evolutionary tracks from the FRUITY repository (Cristallo et al. 2011) for ZAMS masses of 1.3, 1.5, 2.0 and 2.5  $M_{\odot}$ , respectively. Portions of the tracks with recursive third dredge-up events are marked in red. The black dashed line shows the tip of the early-AGB phase. Long-dashed red line: onset of dredge-up episodes. Typical error bars are shown in the upper left corner.

In Paper I a high  $^{16}\text{O}/^{17}\text{O}$  ratio was shown to be an indicator of a low main-sequence mass. Models predict  $^{16}\text{O}/^{17}\text{O}=1000$  stars with  $1.5M_{\odot}$ , and  $^{16}\text{O}/^{17}\text{O}=2650$  for  $1M_{\odot}$  (Paper I). We show in Figure 8 the  $^{16}\text{O}/^{17}\text{O}$  ratio against the  $^{12}\text{C}/^{13}\text{C}$  ratio for our sample stars. We conclude from that plot that the majority of our sample consists of stars of 1.5 to  $2.5M_{\odot}$ , which have not yet experienced third dredge-up as indicated by their low isotopic ratio of carbon. Since our sample was randomly selected among the small-amplitude LPVs, we propose that the above mentioned mass range is typical for SRbs/Lbs in the solar neighborhood.

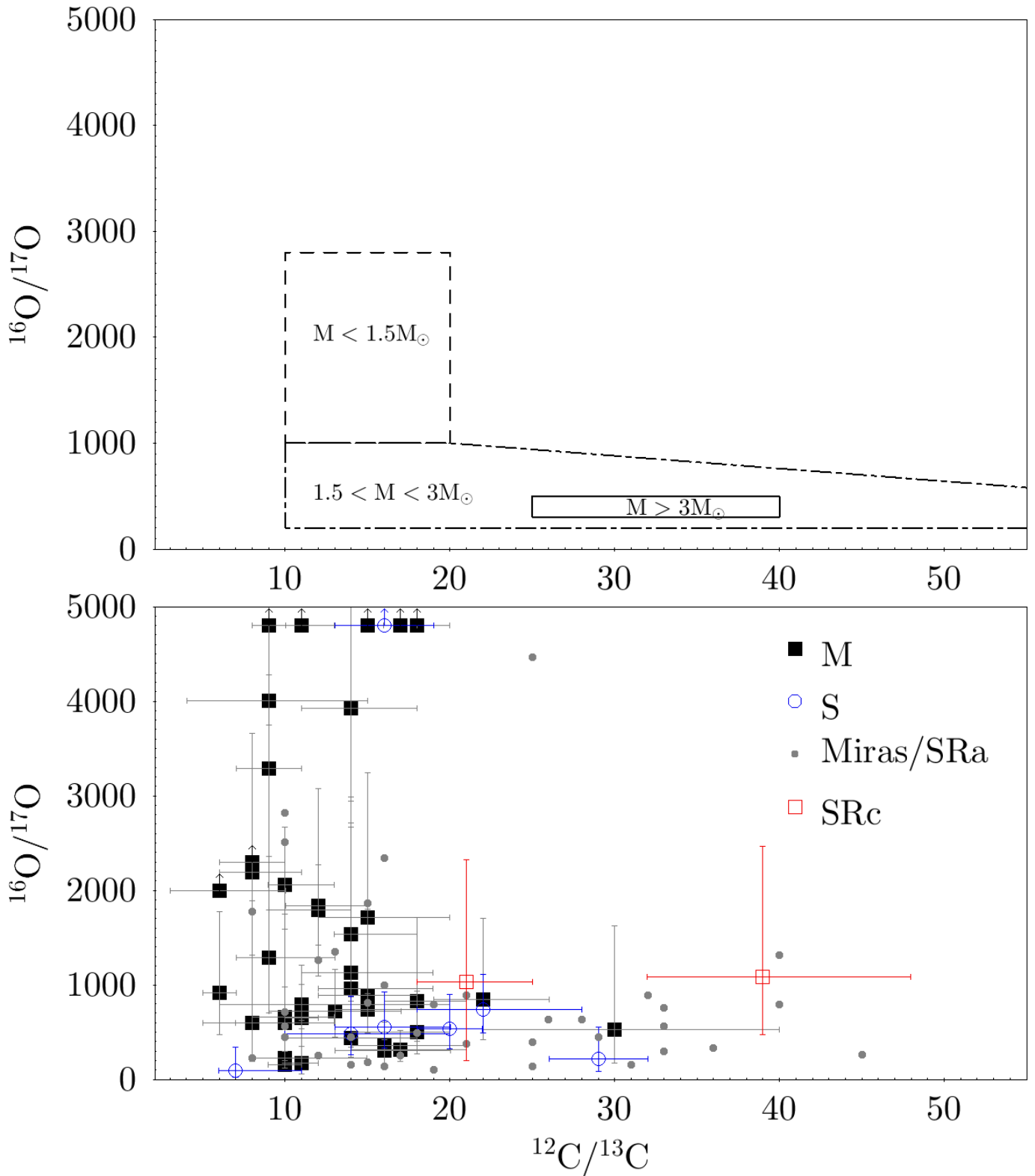


**Figure 8.**  $^{16}\text{O}/^{17}\text{O}$  vs.  $^{12}\text{C}/^{13}\text{C}$  for oxygen-rich LPVs. Filled boxes: SRbs of spectral type M (this paper); open circles: SRbs of type S (this paper); small filled circles: Miras and SRa variables (Paper I). Data points with arrows denote lower limits. The box marked by dashed lines indicates the location of stars below  $1.5M_{\odot}$  according to stellar evolution models, the area surrounded by dashed-dotted lines of stars between  $1.5$  and  $3M_{\odot}$ . See text and Paper I for details.

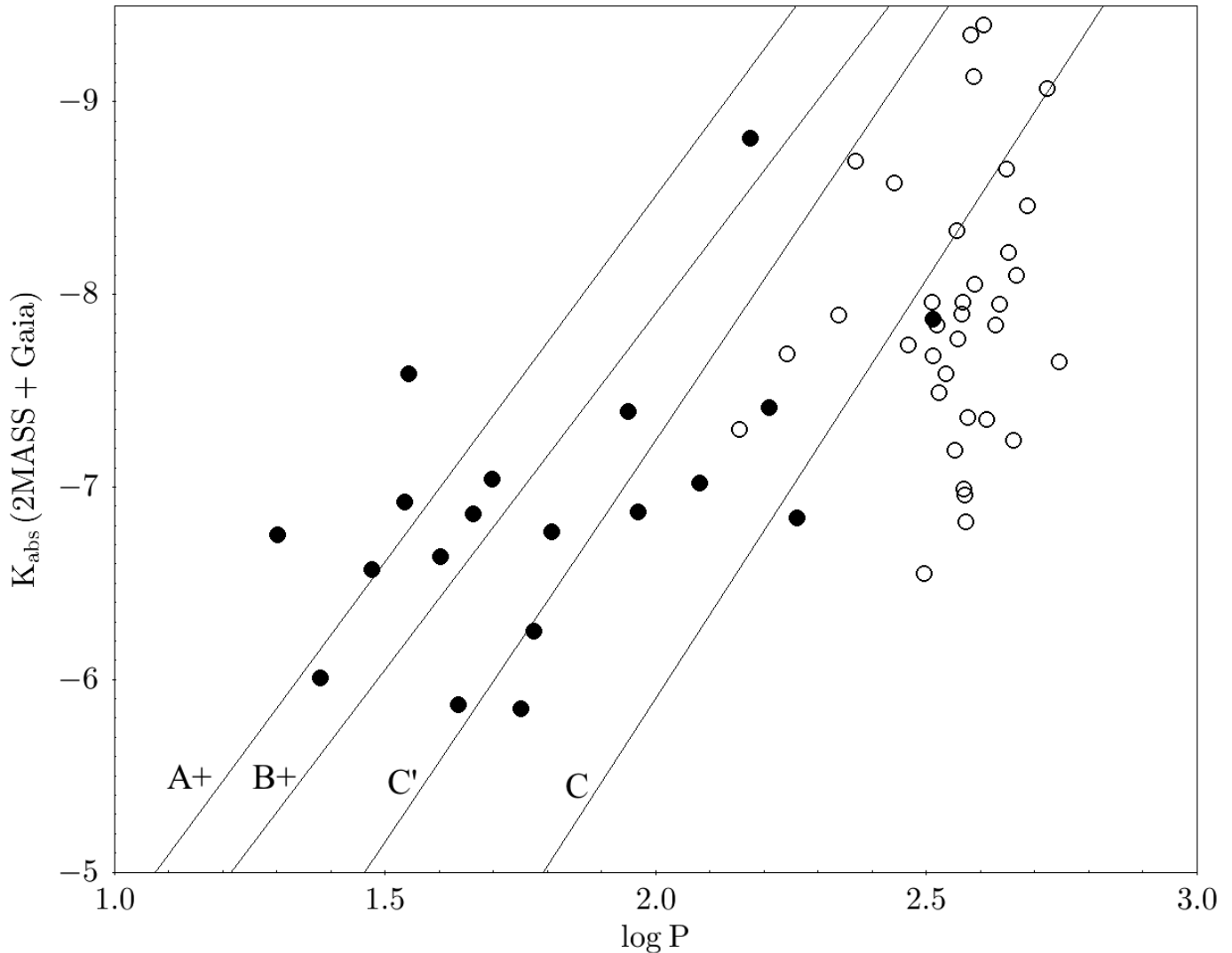


**Figure 9.** logP-K-diagram for the LPVs from Paper I (open circles) and this paper (filled symbols). Lines mark the logP-K-sequences derived from LMC data by *Ita et al. (2004)* corrected for the LMC distance (*de Grijs et al. 2017*). Sequences A+, B+, C', and C are shown from left to right.

The miras and SRa variables from Paper I have been included in Figure 8 with small symbols. The bulk of the SRbs are located immediately to the left of the Miras and SRas. Both groups of stars occupy the same range in  $^{16}\text{O}/^{17}\text{O}$  and hence cover the same range of mass. Third dredge-up shifts the stars to the right in this diagram. This suggests that SRbs are progenitors of miras/SRas. The SRbs have not yet reached the thermally pulsing AGB.

The two SRcs in our sample do not differ significantly from the rest of our sample. Note that we could not compute luminosities for these two stars owing to the lack of a reliable Gaia parallax. Therefore, we cannot test their supergiant nature in this way. Their  $^{12}\text{C}/^{13}\text{C}$  ratios between 20 and 40 are comparable to what has been found for other red supergiants. *Milam et al. (2009)* list a range of 8 to 46 for these luminous stars. The  $^{16}\text{O}/^{17}\text{O}$  ratio is close to 1000 for both stars. Studies on the oxygen isotopes in supergiants are rare. Values between 500 and 850 have been reported (*Harris, & Lambert 1984a; Geballe et al. 1977*).

The evolutionary sequence suggested by the previous arguments is further supported by the location of the sample from this paper and the one from Paper I in a logP-K-diagram (Figure 9). A large number of studies exist today revealing the presence of several parallel pulsation sequences in such a diagram. We indicated in Figure 9 the ones derived by *Ita et al. (2004)* from LMC data. AGB stars pulsate in the fundamental mode (*Wood 2015*, sequence C) and overtones to the left the fundamental in this diagram. *Trabucchi et al. (2019)* pulsation models for a  $1.5 M_{\odot}$  star have evolution tracks from the lower left to the upper right in this diagram, switching pulsation modes from overtone

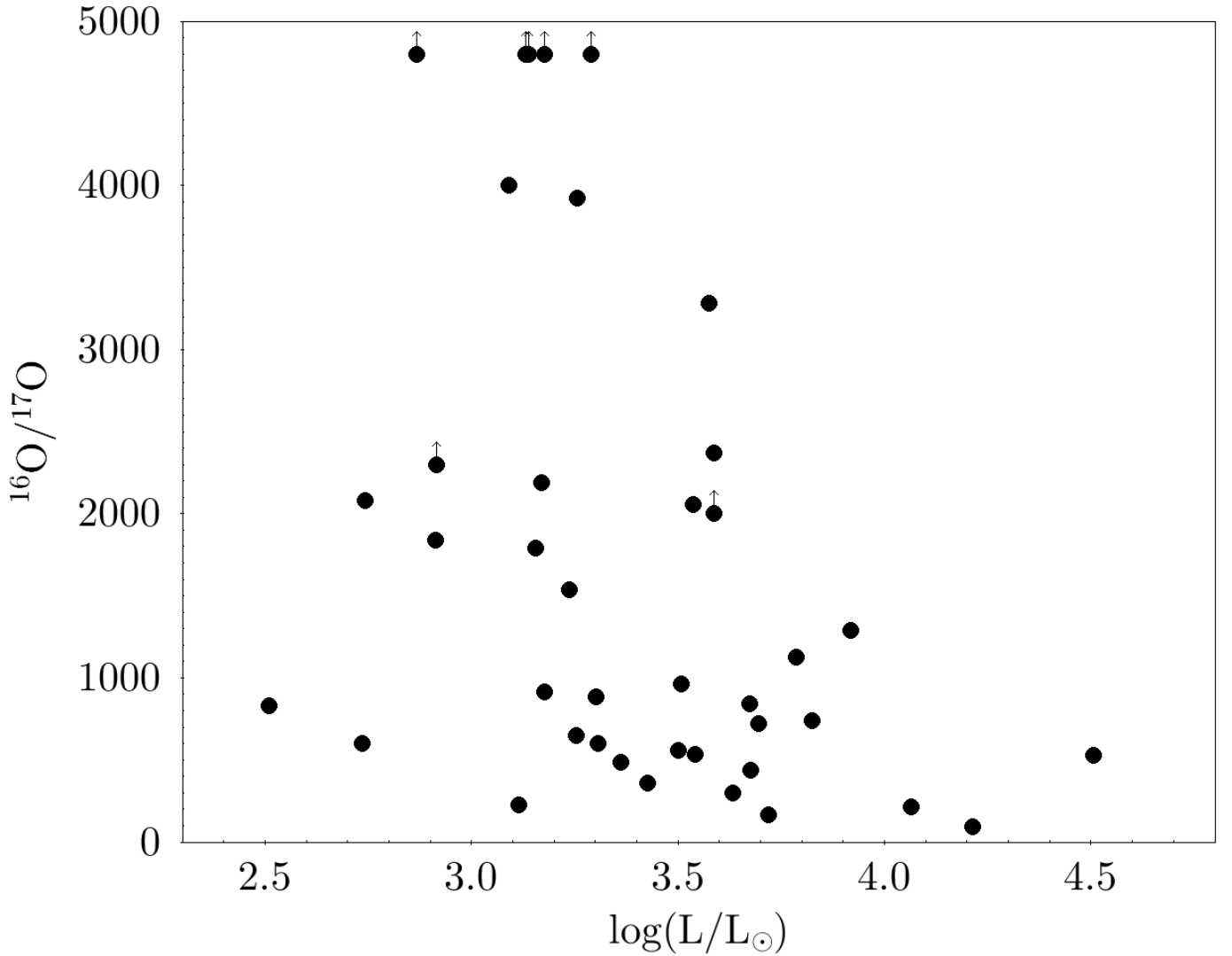


**Figure 10.**  $^{16}\text{O}/^{17}\text{O}$  ratio against luminosity. The sample shown here is limited to those objects for which a Gaia distance was available. Data points with arrows denote lower limits.

to fundamental. This is consistent with Figure 9 where the low-mass SRb stars evolve from lower left to upper right to become the low-mass miras of Paper I.

Our sample includes also a group of 11 stars with main-sequence masses around  $1 M_{\odot}$  or less according to their  $^{16}\text{O}/^{17}\text{O}$  ratios. Note that among these stars there are three with a very high  $^{16}\text{O}/^{17}\text{O}$  ratio. In such a case, the measured  $\text{C}^{17}\text{O}$  lines are already very weak, and while the order of magnitude of the ratio is likely correct, the exact value is very uncertain. We show these points as limits. Among these stars with very high  $^{16}\text{O}/^{17}\text{O}$  ratios is the S-type star DT Psc discussed in the next section. There is only one mira with a comparably high  $^{16}\text{O}/^{17}\text{O}$ , namely U Ori (Paper I).

The  $^{16}\text{O}/^{17}\text{O}$  ratio is shown as a function of the luminosity in Figure 10. No clear trend between these two quantities is visible. This complies with theoretical predictions, as, on the one hand, luminosity is dependent on He core mass, which is, as noted above, independent of the total mass in the case of low-mass stars. As a consequence, luminosity is dependent on the evolutionary stage along the AGB. On the other hand, the  $^{16}\text{O}/^{17}\text{O}$  ratio depends on the total stellar mass, but should stay constant during AGB evolution except for the case of extra-mixing being active during that phase. At the highest luminosities, we only find low values of  $^{16}\text{O}/^{17}\text{O}$ , i.e. only high mass stars, as expected from the models.

In Figure 11 the  $^{16}\text{O}/^{17}\text{O}$  and  $^{16}\text{O}/^{18}\text{O}$  ratios are compared. Solar values are shown (dashed lines) as is the value for  $^{16}\text{O}/^{18}\text{O}$  expected after the first dredge-up (dash-dot line, see Lebzelter et al. 2015a). Stars in the lower left corner,

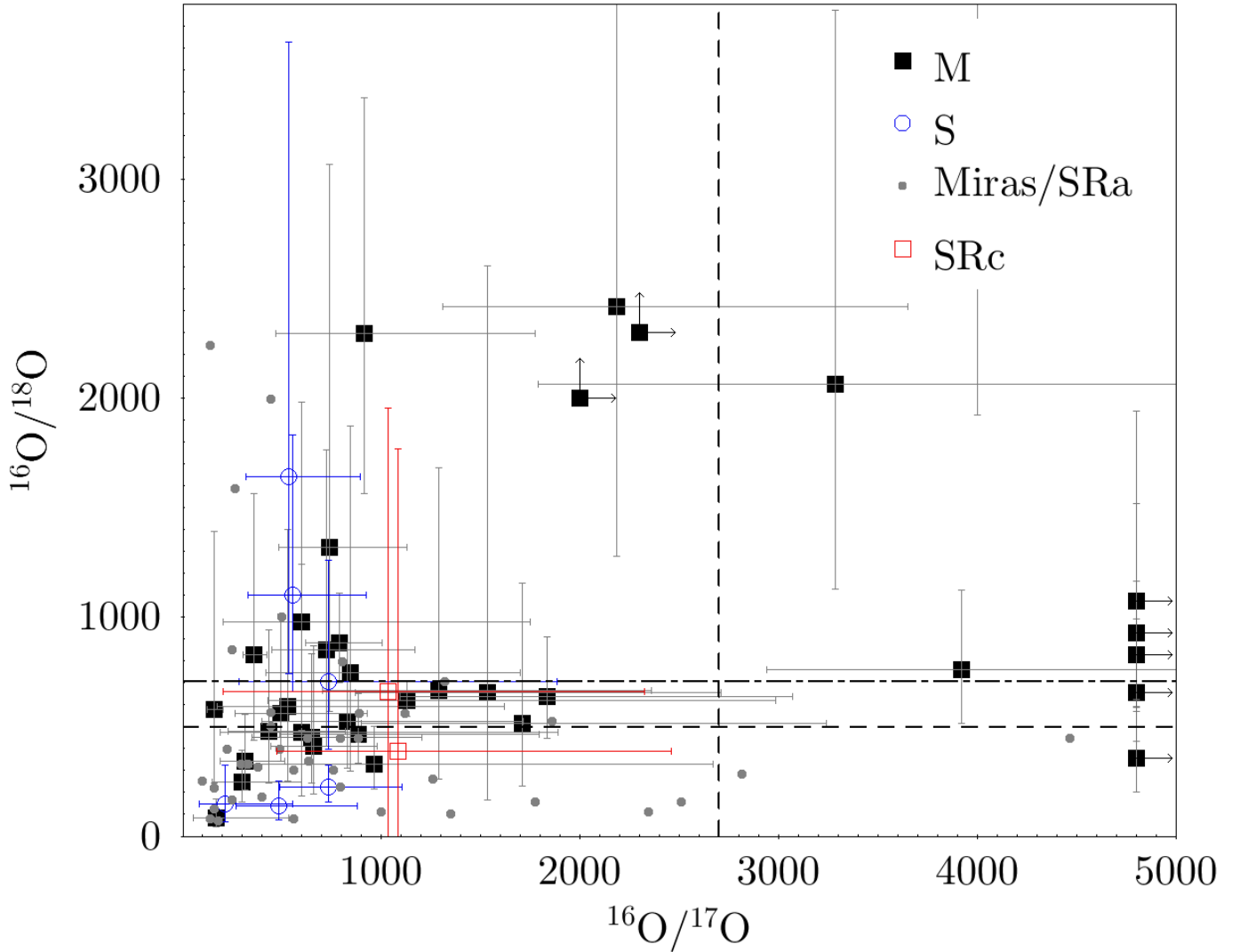


**Figure 11.**  $^{16}\text{O}/^{17}\text{O}$  vs.  $^{16}\text{O}/^{18}\text{O}$  for oxygen-rich LPVs. Same symbols as in Figure 8. Data points with arrows denote lower limits. The dashed lines indicate the solar values. The dashed-dotted line marks the  $^{16}\text{O}/^{18}\text{O}$  expected after first dredge-up.

below the first dredge-up value and to the left of the solar  $^{16}\text{O}/^{17}\text{O}$  line, comply with model expectations. They are more massive than the sun, therefore younger, and their lower  $^{16}\text{O}/^{18}\text{O}$  ratio suggests their formation from material enhanced in  $^{18}\text{O}$  owing to the galacto-chemical evolution (Prantzos et al. 1996; Kobayashi et al. 2011; Lebzelter et al. 2015a). A similar result was found for the bulk of the miras and SRAs in Paper I.

Stars outside of this box require a different interpretation. For those with  $^{16}\text{O}/^{17}\text{O} > 3000$  we may tentatively guess that they have masses of the order of  $1 M_{\odot}$ . As far as Gaia parallaxes are available, we see from Figure 10 that they have low luminosities and had probably not experienced a third dredge-up yet (Figure 7). If these stars are older than the sun, their primordial  $^{16}\text{O}/^{17}\text{O}$  ratio should have been higher following galacto-chemical evolution models which predict a steep increase in the  $^{16}\text{O}/^{17}\text{O}$  ratio in the galaxy for ages older than the sun Prantzos et al. (1996, Figure 4a).

If this scenario is correct, they should have large  $^{16}\text{O}/^{18}\text{O}$  values as well. We see in Figure 11 that two, maybe three stars comply with this condition. The  $^{16}\text{O}/^{18}\text{O}$  values of the other stars with  $^{16}\text{O}/^{17}\text{O} > 3000$  are close to the first dredge-up value computed for a star of similar primordial composition as the sun. These objects do not comply with predictions from stellar evolution models as either their  $^{16}\text{O}/^{17}\text{O}$  ratio is too high or their  $^{16}\text{O}/^{18}\text{O}$  ratio is too low. At this point we can only guess that their primordial composition deviated from the average ISM composition at the time of their formation, e.g. as the result of a nearby supernova.

**Table 6.** Summary of the Properties and Isotopic Ratios of the S-stars Investigated.

HD	Variable star name	Spectral type	Tc?	Li?	this paper/Paper I			Literature <sup>a</sup>	
					<sup>12</sup> C/ <sup>13</sup> C	<sup>16</sup> O/ <sup>17</sup> O	<sup>16</sup> O/ <sup>18</sup> O	<sup>12</sup> C/ <sup>13</sup> C	<sup>16</sup> O/ <sup>17</sup> O
7351	DT Psc	S3+/2-	no <sup>b</sup>	no	16 <sup>+3</sup> <sub>-3</sub>	>8000	...	12, 24	2500, 3000
22649	BD Cam	S3.5/2	no <sup>c</sup>	no	14 <sup>+6</sup> <sub>-4</sub>	486 <sup>+394</sup> <sub>-217</sub>	140 <sup>+115</sup> <sub>-63</sub>	25, 34, 55	350, 2250
30959	o <sup>1</sup> Ori	M3SIII	yes <sup>d</sup>	no	16 <sup>+5</sup> <sub>-2</sub>	360 <sup>+64</sup> <sub>-54</sub>	827 <sup>+734</sup> <sub>-389</sub>	10, 18, 25	480, 925
49368	V613 Mon	S3/2	no <sup>e</sup>	no <sup>k</sup>	16 <sup>+4</sup> <sub>-3</sub>	556 <sup>+372</sup> <sub>-223</sub>	1103 <sup>+732</sup> <sub>-440</sub>	14	430
58521	Y Lyn	M6S	yes <sup>c</sup>	no	39 <sup>+9</sup> <sub>-7</sub>	1087 <sup>+1378</sup> <sub>-608</sub>	387 <sup>+256</sup> <sub>-154</sub>	27, 43	560
64332	NQ Pup	S4.5/2	yes <sup>f</sup>	...	20 <sup>+2</sup> <sub>-2</sub>	534 <sup>+359</sup> <sub>-215</sub>	1643 <sup>+1985</sup> <sub>-899</sub>	18	400
163990	OP Her	M6S	yes <sup>d</sup>	no	7 <sup>+4</sup> <sub>-3</sub>	435 <sup>+386</sup> <sub>-205</sub>	478 <sup>+461</sup> <sub>-234</sub>	11, 20, 21	329, 360, 850
198164	CY Cyg	SC2/7.5	yes <sup>b</sup>	yes	7 <sup>+4</sup> <sub>-1</sub>	94 <sup>+248</sup> <sub>-69</sub>	...	5, 5.6	350, 620
216672	HR Peg	S4+/1+	yes <sup>c</sup>	yes	22 <sup>+6</sup> <sub>-4</sub>	737 <sup>+368</sup> <sub>-245</sub>	223 <sup>+102</sup> <sub>-70</sub>	63, 71	2400
218634	GZ Peg	M4S	no <sup>g</sup>	no	11 <sup>+1</sup> <sub>-1</sub>	169 <sup>+363</sup> <sub>-115</sub>	86 <sup>+85</sup> <sub>-43</sub>	30	...
260297	DY Gem	S8,5	no <sup>e</sup>	...	56 <sup>+23</sup> <sub>-16</sub>	733 <sup>+1152</sup> <sub>-448</sub>	704 <sup>+553</sup> <sub>-309</sub>	30	570
	TV Aur	S5/6	yes <sup>e</sup>	yes	29 <sup>+3</sup> <sub>-3</sub>	213 <sup>+339</sup> <sub>-131</sub>	149 <sup>+176</sup> <sub>-81</sub>	5	240
1967	R And	S5-7/4-5e	yes <sup>h</sup>	no	40±15	1320±300	710±150	24, 33	...
29147	T Cam	S5-6/5e	yes <sup>b</sup>	yes	31±10	160±70	220±90	...	...
185456	R Cyg	S4-8/6e	yes <sup>b</sup>	yes	29±10	450±120	500±200	24, 26, 34	860
187796	χ Cyg	S6-9/1-2e	yes <sup>b</sup>	no	36±4	330±100	330±70	39, 40	...
209890	RZ Peg	SC5-9/9-e	yes <sup>b,j</sup>	yes	9±5	...	...	12	...

(a) References see Table 4 and Table 5 of Paper I. (b) Little et al. (1987). (c) Smith, & Lambert (1988). (d) Lebzelter, & Hron (1999). (e) Smith & Lambert (1990). (f) Shetye et al. (2018). (g) Van Eck et al. (1998). (h) Jorissen et al. (1993). (j) Vanture et al. (2007) give  $\log N(\text{Tc}) \leq 0.4$ . (k) No Li line visible in ELODIE library spectrum (Prugniel et al. 2007). The final five objects are miras/SRas from Paper I. Information on the presence of a Li line is from Vanture et al. (2007).

One star in our SRb sample, RZ Ari, shows a high <sup>16</sup>O/<sup>18</sup>O combined with a comparably low <sup>16</sup>O/<sup>17</sup>O. The latter suggests a mass higher than the sun. For massive AGB stars,  $\gtrsim 6 M_{\odot}$ , hot bottom burning decreases <sup>12</sup>C/<sup>13</sup>C and strongly increases <sup>16</sup>O/<sup>18</sup>O (see Paper I). RZ Ari has a moderate luminosity, and we can thus exclude HBB or extra-mixing on the AGB affecting the surface composition. We may speculate that the composition of RZ Ari results from mass transfer in a binary system. The star had been part of a study of unresolved problem stars from the Hipparcos catalogue, i.e. stars with a suspected binarity, but Speckle interferometry did not produce conclusive results (Mason et al. 1999). Among the miras, the star S Ori shows a very similar isotopic pattern. Additional candidates both from Paper I and from the present sample have large error bars and are thus not included in this discussion. We will come back to RZ Ari in 5.3.

We conclude the discussion with the star SW Vir. This object has the highest luminosity in our sample and is clearly offset from the rest of the SRbs (Figure 7). Taking its luminosity at face value, the star is either a supergiant or a massive AGB star ( $M > 6 M_{\odot}$ ). Looking at the isotopic ratios, a red supergiant, that was a slow rotator on the main sequence, is the preferred hypothesis. However, SW Vir shows a variability more typical of an AGB star than a supergiant. With its period of 150 d and  $K_{abs}$ , computed from the Gaia distance combined with the 2MASS  $K$  magnitude, the star is located on overtone pulsation sequence A+ in Figure 9. The light amplitude of more than 1 mag according to the GCVS is highly uncommon for a star on A+ (Kiss, & Bedding 2003) raising doubts on the derived luminosity. We note that the Gaia DR2 parallax is a factor of 2 smaller than the earlier Hipparcos measurement. While we cannot exclude a supergiant classification from the existing data, the luminosity of SW Vir may indeed be considerably smaller.

## 5.2. S-type stars

Stars of spectral type S show a strong enhancement of *s*-process elements on their surface. There are two processes known to form S-type stars, either by third dredge-up on the AGB (intrinsic S-stars) or by mass transfer from a further evolved companion in a binary system (extrinsic S-stars, see for additional discussion Vanture et al. 2007). The intrinsic classification depends on detection of the radioactive *s*-process element Tc. Since the half-life time of its



longest-living isotope is only  $2 \times 10^6$  yr, any Tc detectable on the surface must have been produced and dredged to the surface recently. In contrast, binarity is the criterion to identify an extrinsic S-star (Brown et al. 1990).

Intrinsic S-stars must have already experienced at least one third dredge-up event. This should be detectable in the  $^{12}\text{C}/^{13}\text{C}$  ratio. A reasonable expectation is that the intrinsic S-stars will have  $^{12}\text{C}/^{13}\text{C}$  intermediate between values for tip AGB oxygen-rich stars ( $8 \lesssim ^{12}\text{C}/^{13}\text{C} \lesssim 45$ , Paper I) and carbon stars ( $30 \lesssim ^{12}\text{C}/^{13}\text{C} \lesssim 70$ , Lambert et al. 1986). The data on the S and MS stars in our sample and in Paper I are summarized in Table 6. Drawing on the work of Vanture et al. (2007) we have added information on the presence of Tc (column 4) and on Li (column 5). Lithium is destroyed by H-burning on the main sequence and should not be present after the first dredge-up. However, observations clearly indicate its presence all along the RGB (Charbonnel et al. 1999; Lebzelter et al. 2012). Extra-mixing on the RGB can be invoked to explain the Li. Li also can be produced in stars with masses above  $3 M_{\odot}$  by HBB via the Cameron-Fowler-mechanism. Examples for the latter process have been found in Li-rich, luminous S-stars in the Magellanic Clouds (Smith, & Lambert 1989).

Our sample includes 15 S and MS stars and two SC stars. 12 of them show Tc lines and are thus intrinsic S-stars. Among them is  $\text{o}^1$  Ori, a star that is also known to be a binary (e.g. Lebzelter, & Hron 1999). The average  $^{12}\text{C}/^{13}\text{C}$  ratio of this group is 20, consistent with a mild enhancement of  $^{13}\text{C}$  by third dredge-up. However, the scatter among the intrinsic S-stars is quite large. The two SC stars in this group show a much lower value of 7, which indicates a post first dredge-up composition. Abia et al. (2017) have pointed out that SC stars show a very peculiar abundance pattern in general, possibly close to barium stars (Dominy et al. 1986), which are binaries. In this scenario, the presence of Tc is difficult to understand. We note that Vanture et al. (2007), using measurements by Abia, & Wallerstein (1998), give only upper limits for Tc in our two SC stars, CY Cyg and RZ Peg, casting doubt on their classification as intrinsic S-stars. However, Jorissen et al. (1998) did radial velocity monitoring for the two stars and could not find convincing evidence for orbital motion.

Removing the SC stars from the intrinsic S-stars leaves only OP Her and NQ Pup with a low carbon isotopic ratio in this group. In both cases, previous papers give similar or somewhat higher numbers. Clearly OP Her and NQ Pup show only a mild enhancement of  $^{13}\text{C}$ , if at all. Alternatively, extra-mixing may have occurred during the AGB evolution of these stars (Lebzelter et al. 2008), which could have reduced their carbon isotopic ratio.

The five S-stars without Tc in our sample have  $^{12}\text{C}/^{13}\text{C}$  ratios between 7 and 23. Results from the literature for these stars give values between 12 and 55. This suggests that this group consists of stars before and after the onset of third dredge-ups. In the latter ones the number of dredge-ups or the mixing efficiency may have been too low to bring a detectable amount of Tc to the surface.

Besides Tc, the element Nb can be used to discriminate between intrinsic and extrinsic S-stars (e.g. Neyskens et al. 2015). Extrinsic S-stars should show an enhancement of Nb, while intrinsic S-stars should be depleted. For five stars in our sample we found measurements of Nb abundance in the literature, namely, BD Cam, V613 Mon, DT Psc, HR Peg, and NQ Pup (Neyskens et al. 2015; Karinkuzhi et al. 2018). In all five cases, the classification derived from the presence or absence of Tc is confirmed.

There is no correlation between  $^{12}\text{C}/^{13}\text{C}$  and the presence of Li. The occurrence of Li and Tc in one star may be an indicator of an intermediate-mass star with proper conditions for HBB in its interior. There are two candidates in our sample, TV Aur and T Cam, which not only show both elements but also have a low  $^{16}\text{O}/^{17}\text{O}$  ratio. These stars would then be higher-mass AGB stars. This is supported by the high luminosity for TV Aur (Table 2). In the event of hot bottom burning  $^{16}\text{O}/^{18}\text{O}$  is expected to be large, but this is not so for either star.

Except for DT Psc, the  $^{16}\text{O}/^{17}\text{O}$  ratios of the S-type stars are around or below 1000, suggesting masses above  $1.5 M_{\odot}$ . There is no systematic difference between intrinsic and extrinsic S-stars. To explore the relation between carbon and oxygen isotopes and the two classes of S-stars conclusively, a study on a larger sample of objects is necessary.

### 5.3. The role of LPVs in the cosmic matter cycle

Presolar grains, i.e. dust grains that survived the formation process of the solar system without modification and are found in pristine meteorites, are indicators of the various contributors to the cloud from which the sun formed (Zinner 1998). The majority of the oxygen-rich grains are believed to originate in AGB stars because of the isotopic signature they show. In Paper I we compared the oxygen isotopic ratios of miras and SRAs with collected data for presolar grains from Nittler et al. (2008). In this comparison it is important to remember that the contributors of dust to the presolar nebula came from stars that had an AGB phase at least 5 billion years ago.

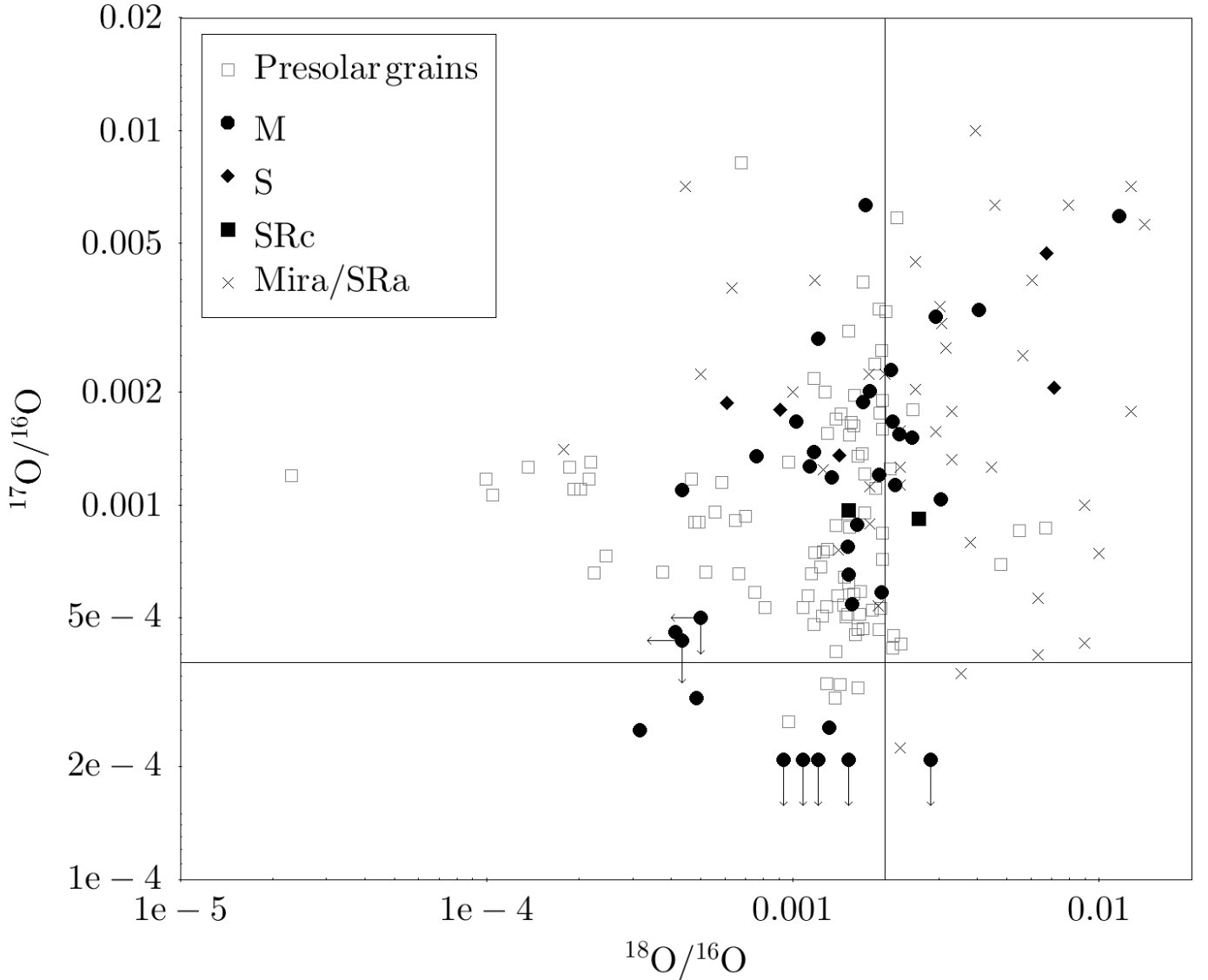


**Figure 12.**  $^{17}\text{O}/^{16}\text{O}$  vs.  $^{18}\text{O}/^{16}\text{O}$  comparing results from AGB stars with presolar grains (open boxes). Filled circles and diamonds mark M- and S-type variables from this paper, respectively. Filled boxes refer to the two SRc in our sample. Crosses mark miras and SRAs from Paper I. The two lines mark the isotopic ratios for the sun. Isotopic ratios are plotted reverse compared to the rest of the paper. Symbols with arrows mark upper limits.

In Figure 12 we plotted the two oxygen isotopic ratios for a sample of presolar grains, the sample from Paper I, and our current sample. The isotopic ratios have been inverted in this discussion to comply with the standard notation used for presolar grains. The bulk of the miras and SRAs have larger than solar  $^{18}\text{O}/^{16}\text{O}$  values (Paper I). This was expected as most of these AGB stars must have formed later than the contributors of the presolar grains with their  $^{18}\text{O}/^{16}\text{O}$  ratio modified by the galactic evolution. The majority of the stars presented in this paper, SRBs and Lbs, are found much closer to the solar value and occupy almost the same area in the diagram as the so-called group 1 presolar grains. This difference between the Paper I stars and the SRBs can be explained by the depletion of  $^{18}\text{O}$  during stellar evolution. The  $^{12}\text{C}/^{13}\text{C}$  ratio we find in the SRBs is typically around 10 or lower (Figure 8). Such values are an evidence of RGB extra-mixing and implies temperatures of 23 to 24 MK in the area reached by the first dredge-up. At such conditions,  $^{18}\text{O}$  is expected to be depleted as it is seen in our observations. In  $^{17}\text{O}/^{16}\text{O}$ , an identical range is covered by this group of stars as by the presolar grains.

As pointed out by Nittler (2009), stellar evolution models attribute group 1 stars to the dusty winds from O-rich AGB stars, and our observations nicely confirm this. When simply associating the abscissa in this diagram with an

indicator for the age of a star, many members of our sample would have an age between the sources of the presolar grains and the sun. Thus, they should have a mass somewhat above  $1 M_{\odot}$  with the associated  $^{17}\text{O}/^{16}\text{O}$  ratios as seen in Figure 12 (compare Section 5.1). In accordance with this picture, the SRBs in the upper right corner of Figure 12 show  $^{18}\text{O}/^{16}\text{O}$  ratios similar to the younger miras and SRAs from Paper I. However, we have to be aware that the primordial amounts of the oxygen isotopes are not equally distributed within our Galaxy resulting in scatter due to the different places of origin of our sample stars. Wilson, & Rood (1994) showed that the interstellar  $^{18}\text{O}/^{16}\text{O}$  ratio rather continuously changes by a factor of two between the Galactic centre and the local ISM. Furthermore, stars may have been enriched during their formation by material from massive stars (Wouterloot et al. 2008).

There are a few stars that do not follow the above-mentioned general trend: We notice four stars with  $^{18}\text{O}/^{16}\text{O}$  close to solar but  $^{17}\text{O}/^{16}\text{O}$  subsolar, i.e. one would assume that these stars should have a lower mass than the sun, but they were formed at a similar time as the majority of our sample. There is also one mira found in this part of the diagram. We mentioned this strange group of objects already in Section 5.1 and speculated about a potential modification of their composition by a nearby supernova exploding before their birth. The few grains visible close to the solar isotopic ratios, named group 3, are associated with an origin in the interstellar medium. However, it may be that such grains stem from this potentially rare group of stars.

One star of our sample, RZ Ari, shows oxygen isotopic ratios similar to grains in group 2. That group can be explained by AGB stars experiencing extra-mixing on the AGB or hot bottom burning (both processes reduce their  $^{18}\text{O}/^{16}\text{O}$ , see Paper I). The  $^{17}\text{O}/^{16}\text{O}$  ratio as well as the derived luminosity do not favor a mass  $> 3 M_{\odot}$ . A strong Li line, found by Merchant (1967) has its origin probably in processes on the RGB (e.g. Lebzelter et al. 2012). In Paper I we noted that the star SV Cas belongs to this group, too. These two targets are interesting for further studies on the phenomenon of extra-mixing on the AGB. We may speculate that the four stars at similar  $^{18}\text{O}/^{16}\text{O}$  but lower  $^{17}\text{O}/^{16}\text{O}$  are also affected by extra-mixing.

## 6. CONCLUSIONS

In this paper we presented isotopic ratios of the two key elements C and O for a sample of mainly O-rich long-period variables with small amplitudes. We demonstrated that these isotopic ratios can be measured accurately with the classical curve-of-growth method. Comparison with other methods in the form of literature values and model spectra computed in the course of this study illustrates that the various methods lead to similar results except for very cool and highly variable objects. Our comparison focused on O-rich stars only. Due to the low excitation temperatures of the cool carbon stars, an extension of this technique to these stars is a complex undertaking and beyond the scope of the present work.

Combined with the results from Paper I, our study allows a broad view of the isotopic composition of the whole range of LPVs. The three ratios  $^{12}\text{C}/^{13}\text{C}$ ,  $^{16}\text{O}/^{17}\text{O}$ , and  $^{16}\text{O}/^{18}\text{O}$  are related to the evolutionary state, the mass and the primordial composition of these stars and thus allows insight into these key parameters. We find that most small-amplitude LPVs have main-sequence masses between  $1.3$  and  $2.5 M_{\odot}$ . An evolutionary scenario from these small-amplitude variables to the large amplitude miras, suggested also by their location in the HRD and in a period-luminosity diagram, is in very good agreement with the findings from the isotopic ratios of C and O.

The majority of the isotopic patterns observed in SRVs and Miras complies well with model predictions. They can be explained in terms of mass and evolutionary differences and signatures of galacto-chemical evolution, so that we can attribute a mass range, an age, and an evolutionary phase to the various groups among the LPVs. Results are consistent with conclusions derived from comparison with stellar evolution tracks and pulsational properties.

Finally, we contrasted our results to the findings from presolar grains. Grain data on isotopic ratios reflect the composition of dust in the pre-solar nebula and should provide an imprint of the dust-producing stars contributing to the origin of the solar system. The LPVs studied here and in Paper I agree well with presolar grains in  $^{17}\text{O}/^{16}\text{O}$ , suggesting that the majority of these grains stem from AGB stars in the  $1.3$  to  $2.5 M_{\odot}$  range. While miras and SRAs show an offset from presolar grains in  $^{18}\text{O}/^{16}\text{O}$  (as noted in Paper I), the SRBs and irregular variables investigated in this paper do not show such a shift. We suggest that this is due to a mass difference between the miras and the SRBs sample and as a consequence a depletion of  $^{18}\text{O}$ . A few data points in our comparison do not follow the expectations from standard models and will require further investigation.

## ACKNOWLEDGMENTS

The authors are indebted to Bernhard Aringer for providing access to his model atmosphere code and for his support with computing the synthetic spectra used in this paper. Sharon Hunt provided assistance with the citations, Overleaf, and ORCID. NSF's National Optical-Infrared Astronomy Research Laboratory, which has superseded the National Optical Astronomy Observatory (NOAO), is operated by the Association of Universities for Research in Astronomy under cooperative agreement with the National Science Foundation. KH thanks the NOAO Office of Science for supporting his research. This work made use of data from the European Space Agency (ESA) mission *Gaia* (<https://www.cosmos.esa.int/gaia>), processed by the Gaia Data Processing and Analysis Consortium (DPAC). Funding for the DPAC has been provided by national institutions, in particular the institutions participating in the *Gaia* Multilateral Agreement. This research was facilitated by the SIMBAD database, operated by CDS in Strasbourg, France, and NASA's Astrophysics Data System Abstract Service. We acknowledge with thanks the variable star observations from the AAVSO International Database contributed by observers worldwide and used in this research.

## REFERENCES

- Abia, C., & Wallerstein, G. 1998, *MNRAS*, 293, 89
- Abia, C., Hedrosa, R.P., Domínguez, I., & Straniero, O. 2017, *A&A*, 599, A39
- Aringer, B., Girardi, L., Nowotny, W., et al. 2016, *MNRAS*, 457, 3611
- Bailer-Jones, C. A. L., Rybizki, J., Foesneau, M., et al. 2018, *AJ*, 156, 58
- Bessell, M.S., Castelli, F., & Plez, B. 1998, *A&A*, 333, 231
- Blackwell, D.E. & Shallis, M.J. 1977, *MNRAS*, 180, 177
- Blackwell, D.E., Petford, A.D., Arribas, S., Haddock, D.J., & Selby, M.J. 1990, *A&A*, 232, 396
- Boothroyd, A.I., Sackmann, I.-J., Wasserburg, G. 1994, *ApJ*, 430, L77
- Brown, J. A., Smith, V. V., Lambert, D. L., et al. 1990, *AJ*, 99, 1930
- Charbonnel, C., Brown, J. A., & Wallerstein, G. 1999, *Stsci Symp. Ser.12: Unsolved Problems in Stellar Evolution*, 5
- Cristallo, S., Piersanti, L., Straniero, O., et al. 2011, *ApJS*, 197, 17
- de Grijs, R., Courbin, F., Martínez-Vázquez, C. E., et al. 2017, *SSRv*, 212, 1743
- Dearborn, D. S. P. 1977, *CNO Isotopes in Astrophysics*, 39
- Dominy, J.F., Wallerstein, G., & Suntzeff, N.B. 1986, *ApJ*, 300, 325
- El Eid, M.F. 1994, *A&A*, 285, 915
- Fernie, J. D. 1991, *PASP*, 103, 559
- Gaia Collaboration, Brown, A.G.A., Vallenari, A., Prusti, T., et al. 2018, *A&A*, 616, A1
- Geballe, T. R., Wollman, E. R., Lacy, J. H., et al. 1977, *PASP*, 89, 840
- Guandalini, R., & Busso, M. 2008, *A&A*, 488, 675
- Hall, D.N.B., Ridgway, S.T., Bell, E.A., & Yarborough, J.M. 1979, *Proc. SPIE*, 172, 121
- Harris, M. J., & Lambert, D. L. 1984a, *ApJ*, 281, 739
- Harris, M.J. & Lambert, D.L. 1984b, *ApJ*, 285, 674
- Harris, M.J., Lambert, D.L., & Smith, V.V. 1985, *ApJ*, 299, 375
- Harris, M.J., Lambert, D.L., Hinkle, K.H., Gustafsson, B., Eriksson, K. 1987, *ApJ*, 316, 294
- Hinkle, K.H., Lambert, D.L., & Snell, R.L. 1976, *ApJ*, 210, 684
- Hinkle, K.H., Lebzelter, T., & Straniero, O. 2016, *ApJ*, 825 (Paper I)
- Hoffleit, D. 1964, *Catalogue of Bright Stars*, 3rd edition (Yale University:New Haven).
- Ita, Y., Tanabé, T., Matsunaga, N., et al. 2004, *MNRAS*, 347, 720
- Jorissen, A., Frayer, D. T., Johnson, H. R., et al. 1993, *A&A*, 271, 463
- Jorissen, A., Van Eck, S., Mayor, M., et al. 1998, *A&A*, 332, 877
- Justtanont, K., Barlow, M. J., Blommaert, J., et al. 2015, *A&A*, 578, A115
- Karakas, A.I. & Lattanzio, J.C. 2014, *PASA*, 31, 30
- Karinkuzhi, D., Van Eck, S., Jorissen, A., et al. 2018, *A&A*, 618, A32
- Keenan, P. C. 1942, *ApJ*, 95, 461
- Kerschbaum, F., Lebzelter, T., & Mekul, L. 2010, *A&A*, 524, A87
- Kiss, L. L., & Bedding, T. R. 2003, *MNRAS*, 343, L79
- Kobayashi, C., Karakas, A. I., & Umeda, H. 2011, *MNRAS*, 414, 3231
- Lambert, D.L., Gustafsson, B., Eriksson, K., & Hinkle, K.H. 1986, *ApJS*, 62, 373
- Lattanzio, J., Frost, C., Cannon, R., et al. 1996, *Mem. Soc. Astron. Italiana*, 67, 729
- Lazaro, C., Lynas-Gray, A.E., Clegg, R.E.S., Mountain, C.M., & Zdrozny, A. 1991, *MNRAS*, 243, 62
- Lebzelter, T., & Hron, J. 1999, *A&A*, 351, 533

- Lebzelter, T., & Obbrugger, M. 2009, *Astronomische Nachrichten*, 330, 390
- Lebzelter, T., Lederer, M. T., Cristallo, S., et al. 2008, *A&A*, 486, 511
- Lebzelter, T., Uttenthaler, S., Busso, M., et al. 2012, *A&A*, 538, A36
- Lebzelter, T., Straniero, O., Hinkle, K.H., Nowotny, W., & Aringer, B. 2015a, *A&A*, 578, A33
- Lebzelter, T., Nowotny, W., Hinkle, K. H., et al. 2015b, *Why Galaxies Care About AGB Stars III: A Closer Look in Space and Time*, 283
- Lebzelter, T., Mowlavi, N., Trabucchi, M., et al. 2019, *A&A*, submitted
- Levesque, E. M., Massey, P., Olsen, K. A. G., et al. 2005, *ApJ*, 628, 973
- Little, S. J., Little-Marenin, I. R., & Bauer, W. H. 1987, *AJ*, 94, 981
- Lodders, K., Palme, H., Gail, H.-P. 2009, *Landolt Brnstein* (Springer), 44
- Lord, S.D. 1992, *NASA Technical Memorandum* 103957
- Mason, B. D., Martin, C., Hartkopf, W. I., et al. 1999, *AJ*, 117, 1890
- Meibom, A., Krot, A.N., Robert, F., Mostefaoui, S., Russell, S.S., Petaev, M., Gounelle, M. 2007, *ApJ*, 656, L33
- Merchant, A. E. 1967, *ApJ*, 147, 587
- Milam, S. N., Woolf, N. J., & Ziurys, L. M. 2009, *ApJ*, 690, 837
- Neyskens, P., van Eck, S., Jorissen, A., et al. 2015, *Nature*, 517, 174
- Nittler, L.R. 2009, *PASA*, 26, 271
- Nittler, L. R., Alexander, C. M. O., Gallino, R., et al. 2008, *ApJ*, 682, 1450
- Norton, R.H. & Beer, R. 1976, *J.Opt.Soc.Am.*, 66, 259
- Ohnaka, K. & Tsuji, T. 1996, *A&A*, 310, 933
- Pilachowski, C.A., Hinkle, K.H., Young, M.D., Dennis, H.B., Gopu, A. Henschel, R., Hayashi, S. 2017, *PASP*, 129
- Pojmanski, G., Pilecki, B., & Szczygiel, D. 2005, *AcA*, 55, 275
- Prantzos, N., Aubert, O., & Audouze, J. 1996, *A&A*, 309, 760
- Prugniel, P., Soubiran, C., Koleva, M., et al. 2007, *VizieR Online Data Catalog*, III/251
- Ramstedt, S. & Olofsson, H. 2014, *A&A*, 566, A145
- Richichi, A., Fabbroni, L., Ragland, S., & Scholz, M. 1999, *A&A*, 344, 511
- Ridgway, S.T., Joyce, R.R., White, N.M., and Wing, R.F. 1980, *ApJ*, 235, 126
- Schmidt, M.R., Začs, L., Mikołajewska, J., Hinkle, K.H. 2006, *A&A*, 446, 603
- Schöier, F.L. & Olofsson, H. 2000, *A&A*, 359, 586
- Sharma, K., Prugniel, P., & Singh, H.P. 2016, *A&A*, 585, A64
- Seifahrt, A., Käuff, H.U., Zängl, G., et al. 2010, *A&A*, 524, A11
- Shetye, S., Van Eck, S., Jorissen, A., et al. 2018, *A&A*, 620, A148
- Smith, V.V. & Lambert, D.L. 1986, *ApJ*, 311, 843
- Smith, V. V., & Lambert, D. L. 1988, *ApJ*, 333, 219
- Smith, V. V., & Lambert, D. L. 1989, *ApJL*, 345, L75
- Smith, V.V. & Lambert, D.L. 1990, *ApJS*, 72, 387
- Tokunaga, A. 2002, in 'Allen's Astrophysical Quantities' A.N.Cox, ed., (Springer, Berlin), p. 152.
- Trabucchi, M., Wood, P. R., Montalbán, J., et al. 2019, *MNRAS*, 482, 929
- Tsuji, T. 1991, *A&A*, 245, 203
- Tsuji, T. 2008, *A&A*, 489, 1271
- Van Eck, S., Jorissen, A., Udry, S., et al. 1998, *A&A*, 329, 971
- Vanture, A.D., Smith, V.V., Lutz, J., et al. 2007, *PASP*, 119, 147
- Wallace, L. & Hinkle, K. 1996, *ApJS*, 107, 312
- Wallerstein, G.W. & Morell, O. 1994, *A&A*, 281, L37
- Wilson, T. L., & Rood, R. 1994, *ARA&A*, 32, 191
- Wood, P. R. 2015, *MNRAS*, 448, 3829
- Worthey, G. & Lee, H-C. 2011, *ApJS*, 193, 1
- Wouterloot, J. G. A., Henkel, C., Brand, J., et al. 2008, *A&A*, 487, 237
- Zinner, E. 1998, *AREPS*, 26, 147